October 9, 2017

Master thesis

Quasi-statically driven Otto engine operating simple few-body quantum systems in a 1D infinite square well

Division of Mathematical Physics, Department of Physics, Lund University

Author:
Jim Lundgren

Supervisor:
Stephanie Reimann
Co-supervisor:
Jakob Bengtsson

LUND UNIVERSITY
Faculty of Science

Abstract

In this thesis we investigate the work output from an Otto-engine operating simple, few-body quantum systems under quasi-static driving. We consider 1D systems using the infinite square well as the trapping potential. The aim is to more deeply understand how the working medium of the engine affects the work output, and under which conditions (such as temperatures of the heat reservoirs, particle number etc) a particular working medium is favourable over another. We will first look at how the work output using non-interacting, spin-polarised fermions and bosons differ in the Otto engine. Then, we continue by examining what effect particle number has and how the work output of the non-interacting quantum particles corresponds to that of using a classical, ideal gas as the working medium. After that, a two-body interaction, with a tunable interaction strength is introduced. We will take the interaction to be of the same form as an effective 1D Coulomb interaction for a system under strong cylindrical confinement. We examine how the interacting system compares to the non-interacting one, and what happens when the interaction strength is varied. For the non-interacting case, we find that fermions and bosons can have significantly different work output. The difference will be due to a combination of their respective particle statistics and the monotonically increasing energy level spacings of the infinite square well. Additionally, fermions are seen to be able to have a larger work output than a classical ideal gas, while for bosons, only a system of one or two particles can. Including the two-body interaction, we find that it allows for both fermions and bosons to have a larger work output compared to the non-interacting case. We also see that increasing the interaction strength high enough, fermions and bosons tend to the same work output.

Contents

Acknowledgement

I would like to thank my supervisor Stephanie Reimann for letting me work on this thesis and for the feedback she has given me. Secondly, I would like to thank my co-supervisor Jakob Bengtsson for all the help he has given me whenever I have had any questions and for letting me use his C++ library. Thirdly, I would like to thank all of my officemates throughout the year.

Chapter 1

Introduction

An important topic of classical thermodynamics is that regarding heat engines. The basic idea of an engine is to convert energy from some form to another, in which it can be utilized for a desired purpose. Heat engines specifically, convert energy transferred as heat into energy that is transferred as mechanical work. The petrol-engine of a car is a good example of a heat engine that is used in everyday life. In the petrol-engine, one makes use of the energy released as heat when the fuel is ignited. The heat is partly transformed to mechanical work by making the piston in the cylinder move (which in turn makes the car move). A normal car engine can be described with classical thermodynamics, in terms of the macroscopic quantities involved. But what would happen if we make the engine very small, such that quantum effects become significant? Maybe we could use a large number of these very small engines to improve e.g. work output, efficiency or power compared to a normal-sized car engine? These questions motivate for detailed studies of quantum effects related to heat engines, which is the topic of this thesis.

The idealised version of a petrol-engine is an Otto engine, where the thermodynamic cycle undergone is known as the Otto cycle. In this thesis, we want to consider the Otto cycle applied on few-body systems of quantum particles and see what effects particle statistics and particle interaction have on the engine's work output. Few-body systems are interesting to consider as experimental realisations of heat engines working single-particle systems have been proposed, see e.g. Refs. [1], [2]. We can thus hope that effects and applications of few-body heat engines could be studied in experimental settings in the foreseeable future, making theoretical studies of the topic important.

Elementary quantum systems undergoing the Otto cycle and fundamental concepts related to it have been considered at length, see e.g. Refs. [3] and [4]. Recently, further investigations on quantum systems undergoing the Otto cycle have been done, where the effects of different set-ups have been examined. The effects of trap geometry and particle statistics have been treated in Ref. [5] and effects of particle interaction and sudden-quench driving are considered in Ref. [6].

For this thesis, we will focus on how the work output changes between different non-interacting and interacting few-body quantum systems, when considering quasi-static driving of a one-dimensional (1D) Otto engine. We investigate how the work output depends on the particle type used as working medium, the temperatures of the heat reservoirs in the cycle, and how it varies with the number of particles in the system.

This allows us to assess the specific conditions for which a particular working medium is favourable to another. Additionally, to give us some idea about how engines operating quantum particles compare to "normal" engines, operating classical particles, we will also compare the Otto engine operating non-interacting quantum particles to when it is operating classical, ideal gas particles.

In Ch. 2 we treat the essentials of an Otto engine, looking at the engine operating with classical, ideal particles (Sect. 2.1) and with non-interacting quantum particles (Sect. 2.2). In Ch. 3 we look a bit into the details related to the numerical methods used to deal with the problem at hand, and some relevant theoretical concepts. In Ch. 4 and 5 we present the results found for a working medium of non-interacting respectively interacting particles. The results are discussed and we look at possible explanations of the underlying physics. The thesis ends with an outlook in Ch. 6.

Chapter 2

Theory

In this chapter the ideal Otto engine is described, with Sect. 2.1 serving as the introduction by looking at the cycle undergone by classical systems. As an example we will express the average work output per cycle when the working medium consists of classical, monoatomic, ideal gas particles in 1D. In Sect. 2.2 we turn over to the Otto cycle operating quantum systems, and express the work output for non-interacting, identical particles that exhibit a scaling property in their Hamiltonians.[1]

One important note is that the ideal Otto cycle is undergone *quasi-statically*. A quasi-static process is a thermodynamic process that occurs infinitely slow, such that the system under consideration will be in equilibrium throughout the process. Having the system in equilibrium allows for well-defined macroscopic variables, and therefore one can track the entire change of a system in terms of these variables (see e.g. Ref. [7]). The treatment of the Otto cycle will thus be greatly simplified by it being quasi-static. However, it also necessarily means that the cycle cannot be realised in real life. But, a quasi-static study can be seen as a first step when studying the engine, providing results that should hold in the infinite-time limit of a realistic engine and adding insights about properties of the engine. Additionally, for realistic engines operating the cycle very slowly, we could imagine that the quasi-static predictions would hold to some approximative degree.

2.1 The Otto cycle with classical working media

The concepts of heat and work are central to understanding the Otto cycle. Heat and work are the two ways we can transfer energy into and out of a system. The first law of thermodynamics states that energy is conserved (see any standard physics textbook dealing with thermodynamics or general physics, e.g. Refs. [7], [8], [9]). If then the internal energy is changed in a system, it must be a consequence of heat going into or out of the system and/or work being performed by or on the system. Thus, if the internal energy of the system is denoted by U, infinitesimal heat transferred to the system denoted by $đQ$ and infinitesimal work done by the system denoted by $đW$, an infinitesimal change in the internal energy, dU, is given by

$$dU = đQ - đW \,. \tag{2.1}$$

We use the symbol $đ$ to indicate that the infinitesimal transfer of heat and work are not exact differentials, but path dependent (see e.g. Ref. [10]).

[1] The meaning of a Hamiltonian with a scaling property is discussed later on, in Sect. 2.10b.

The Otto engine can be seen as a heat engine with two *heat reservoirs*, a heat reservoir being a large system such that its temperature does not decrease when coupled to a relatively smaller system. By having two heat reservoirs at different temperatures, we get a heat transfer from the hotter reservoir, with temperature T_h, to the colder reservoir, with temperature T_c. By putting our engine in between the two reservoirs, we can transform some of that heat into work. The leftover heat[2] is dumped into the colder reservoir. The process is illustrated in Fig. 2.1 (left), where the energy flow of a general heat engine with two heat reservoirs is shown.

More specifically, we can represent the Otto engine as a thermodynamic cycle between four states, denoted A, B, C, D. The Otto cycle then runs as $A \to B \to C \to D \to A$, which we sketch in Fig. 2.1 (right) by displaying the pressure versus the volume of the system (called a pressure-volume diagram, or a PV-diagram for short). If we start in state A, our system is coupled to the hot reservoir and in thermal equilibrium with it (such that its temperature, T_A, is $T_A = T_h$). We then decouple the system from the hot reservoir and let it expand, ending up at B. The expansion is done *adiabatically*, which means that no transfer of heat occurs. At B, the system is coupled to the cold reservoir and cooled down. The cooling down occurs as an *isochoric* process, meaning that the volume is kept fixed throughout the process (and hence the volume at B and C are the same, we define $V_c \equiv V_B = V_C$). When state C is reached, the system is in thermal equilibrium with the cold reservoir and has reached the reservoir's temperature (i.e. $T_C = T_c$). The cycle is continued by decoupling the system from the cold reservoir and compressing it adiabatically to D, where it is coupled to the hot reservoir and heated isochorically to A (so the volume at D and A are the same, and we define $V_h \equiv V_D = V_A$).

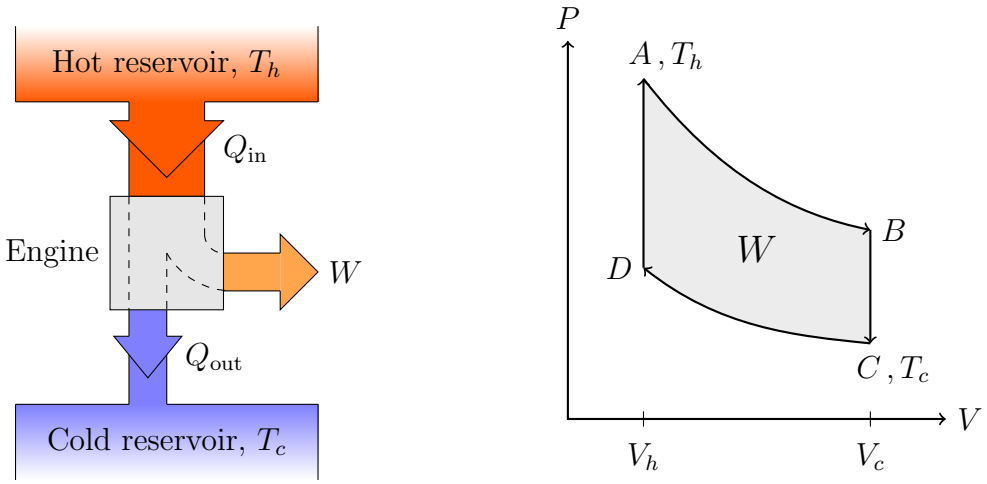

Figure 2.1: (Left) Energy flow of a general heat engine, where Q_{in} is the heat transfer from the hot reservoir, Q_{out} the heat transfer to the cold reservoir and W the work output of the engine. (Right) The PV-diagram of an Otto cycle, where V_h and V_c are the volumes when the system is coupled to the hot reservoir (and fully compressed) respectively when it is coupled to the cold reservoir (and fully expanded).

The system in the Otto cycle is represented as a working medium in some volume that can expand and compress, for example the car engine with the fuel as the working medium and the cylinder-piston as the volume that can expand and compress. As such, we see that

[2]The leftover heat is present as a consequence of entropy, see e.g. Ref. [8].

performing work is related to changing the pressure and volume of our system. We have $đW = P\,dV$, with P being the pressure and V being the volume. The total work output, W, of the cycle is therefore the enclosed area in the PV-diagram (coloured light-grey in Fig. 2.1 (right)).

Another consequence of $đW = P\,dV$ is that during the isochoric processes, $B \to C$ and $D \to A$, no work is performed since the volume is constant throughout these processes. The total work output, W, is given by the sum of the work contribution from the expansion, process $A \to B$, and the work cots of the compression, process $C \to D$. We will refer to these as W_{exp} and W_{comp}, respectively.

Work output for a mono-atomic, ideal gas

Let us now consider a working medium consisting of mono-atomic, ideal gas particles in 1D. Consequently, we can make use of the ideal gas law

$$PV = Nk_BT,$$

where N is the number of particles in the gas and k_B is Boltzmann's constant ($k_B \approx 1.381 \times 10^{-23}$ J/K). We can use the ideal gas law to find the work for the expansion (compression)

$$W_{\text{exp(comp)}} = \int_{V_{h(c)}}^{V_{c(h)}} P\,dV = Nk_B \int_{V_{h(c)}}^{V_{c(h)}} \frac{T\,dV}{V}\,.$$

To proceed, we recall that the expansion and compression strokes are done adiabatically. Using (2.1) with $đQ = 0$, we have $dU = -đW = -P\,dV$. Next, we can make use of the equipartition theorem (see e.g. Ref. [8]), which states that every quadratic degree of freedom contributes (on average) $k_BT/2$ to the internal energy. As we are dealing with a 1D mono-atomic, ideal gas, the energy of each particle is just the translational energy $mv^2/2$. Thus, the equipartition theorem tells us that the internal energy of a system with N such particles is $U = Nk_BT/2$, and hence the change in energy should equal $dU = Nk_B\,dT/2$. Using the ideal gas law to eliminate P we therefore find

$$dU = -P\,dV \;\Rightarrow\; \frac{Nk_B\,dT}{2} = -\frac{Nk_BT\,dV}{V} \;\Rightarrow\; \frac{dT}{T} + 2\frac{dV}{V} = 0\,.$$

This leads to

$$V^2T = \text{constant} \equiv K\,,$$

which we now can use to evaluate the integral above. We find

$$W_{\text{exp(comp)}} = KNk_B \int_{V_{h(c)}}^{V_{c(h)}} \frac{dV}{V^3} = \frac{Nk_B}{2}\frac{K}{V_{h(c)}^2}\left(1 - \frac{V_{h(c)}^2}{V_{c(h)}^2}\right)\,,$$

which we can finally express as

$$W_{\text{exp(comp)}} = \frac{Nk_B}{2}T_{h(c)}\left(1 - \left(\frac{V_{h(c)}}{V_{c(h)}}\right)^2\right)\,. \tag{2.2}$$

Thus, we find that the total work output per cycle, W, is

$$W = W_{\text{exp}} + W_{\text{comp}} = \frac{Nk_B}{2}\left[T_c\left(1 - \left(\frac{V_c}{V_h}\right)^2\right) + T_h\left(1 - \left(\frac{V_h}{V_c}\right)^2\right)\right]\,, \tag{2.3}$$

where the ratio V_c/V_h is known as the compression ratio, $V_c/V_h > 1$.

By looking at (2.2), we see that if we keep increasing the compression ratio, with fixed temperatures and particle number, the expansion work goes to a fixed value while for the compression it blows up to negative infinity. Therefore, in order for the work output to be positive, we must take the expression in brackets of (2.3) to be greater than zero. We find

$$T_h > T_c \left(\frac{V_c}{V_h}\right)^2 , \tag{2.4}$$

which shows that in order to do positive work in the Otto cycle, the lower temperature limit of the hot reservoir does not only depend on the cold reservoir's temperature, but also on the compression ratio. The inequality (2.4) thus gives important information about what parameter space to consider, and what limitations to take into account when constructing an engine.

We could further look into how to maximize the work output (2.3), given a fixed compression ratio while satisfying (2.4). To start, we see that we can obtain a larger work output by adding more particles, and that the work output scales linearly with the particle number, N. For an ideal gas, this is expected, as each particle should behave independently and thus each contribute the same amount to the total work. Secondly, we also see from (2.3) that if we keep T_c fixed we will increase the work output by increasing T_h. This is also expected, as a higher T_h means that more heat is added to the system from the hot reservoir and consequently we obtain a larger work output.

If we instead now let the compression ratio vary, but keep the particle number and temperatures T_h and T_c fixed, how does the work output change? By taking the derivative of (2.3) with respect to the compression ratio, it is found that the maximum occurs when $V_c/V_h = (T_h/T_c)^{1/4}$. We can realise that there should be some maximum by looking at the extreme values of the compression ratio. First, for $V_c/V_h = 1$ there would be no expansion at all, so surely no work is performed here. Second, by continuously increasing V_c/V_h we will at some point contradict the positive work condition in (2.4) and hence reach a point where we have zero work (on the border between having a positive or a negative work output). In between these extremes we thus expect there to be at least one maximum.

2.2 The Otto cycle with quantum working media

In this section we will follow a similar procedure as in the previous section, but treating working media consisting of non-interacting *quantum* particles. Let us begin by considering the system in the Otto engine at the point in the cycle were it is coupled to the hot reservoir, and has been for long enough such that the two are in thermal equilibrium (this corresponds to being in state A in Fig. 2.1 (right)).[3] This implies that the system occupies its internal states, i.e. its energy levels, according to a Boltzmann distribution (see e.g. Ref [8]). Thus, the probability, P_n, to occupy the nth energy level, E_n, at temperature T is given by

$$P_n = \frac{\mathrm{e}^{-E_n/(k_B T)}}{Z} , \tag{2.5}$$

[3]We could just as well have started at the point were the system is coupled to and in thermal equilibrium with the cold reservoir (which corresponds to being in state C in Fig. 2.1 (right)).

where the exponential factor in the numerator is known as the Boltzmann factor and

$$Z = \sum_n \mathrm{e}^{-E_n/(k_B T)} \,,$$

is the partition function [8].

The energy levels of the system are obtained by solving the stationary Schrödinger equation,

$$H\Psi_n(x) = E_n \Psi_n(x) \,, \tag{2.6}$$

where H is the Hamiltonian operator, $\Psi_n(x)$ the nth energy eigenket and E_n the corresponding energy. The general Hamiltonian we will consider, for a system of N particles, has the form

$$H = \sum_{k=1}^{N} \left(-\frac{\hbar^2}{2m} \frac{\partial^2}{\partial x_k^2} + V(x_k) \right) + \frac{1}{2} \sum_{k \neq l} v(x_k, x_l) \,, \tag{2.7}$$

where $V(x_k)$ is the trapping potential for the kth particle and $v(x_k, x_l)$ is a two-body interaction between the kth and the lth particles. We will go into more detail about the trapping potential, the two-body interaction and how we can solve the Schrödinger equation (2.6), and hence obtain the energy levels, in the next chapter.

With the system in thermal equilibrium with the heat reservoir, the average internal energy, U, of the system will be

$$U = \sum_n P_n E_n \,. \tag{2.8}$$

By taking the differential, we find

$$dU = \sum_n E_n \, dP_n + \sum_n P_n \, dE_n \,. \tag{2.9}$$

The two terms on the right-hand side in (2.9) can be identified as infinitesimal heat and work transfer, through (see e.g. Ref. [3])

$$đQ = \sum_n E_n \, dP_n \,, \tag{2.10a}$$

$$đW = -\sum_n P_n \, dE_n \,. \tag{2.10b}$$

In this way, (2.9) takes the same form as in the classical case (2.1), i.e. $dU = đQ - đW$. We can justify the identification of heat transfer done in (2.10a) by considering its relation to the entropy of the system, S. For a quasi-static process, one finds that $đQ = TdS$ (see e.g. Ref. [8]). Thus, heat transfer is due to a change in entropy. Further, the entropy of the system can be expressed as $S = -\sum_n P_n \ln P_n$, which only depends on the occupation-probabilities. Consequently, a change in entropy is solely due to a change in the occupation-probabilities, implying that heat transfer is also solely due to a change in the occupation-probabilities, which is what (2.10a) says. Work must then be the other way of changing the internal energy of the system, i.e. by changing the energy levels as

in (2.10b).[4]

We can use the definitions of heat and work above, to describe the full Otto cycle operating a quantum system. We denote the nth energy level for the isochoric processes (throughout which the energy levels are fixed) by E_n^i, where $i = h, c$ denotes if it is the process starting just after coupling to the hot reservoir, $i = h$, or the cold reservoir, $i = c$. In a similar way, we can denote the occupation-probabilities for the adiabatic processes (throughout which the probabilities are fixed) by P_n^i, with $i = h, c$ denoting the adiabatic process starting just after decoupling from the hot reservoir (i.e. the expansion), $i = h$ or the cold reservoir (i.e. the compression), $i = c$. The Otto cycle in terms of energy and occupation-probability, is plotted in Fig. 2.2 for the nth energy level, using the same labels, A, B, C, D, as for the corresponding states in Fig. 2.1 (right).

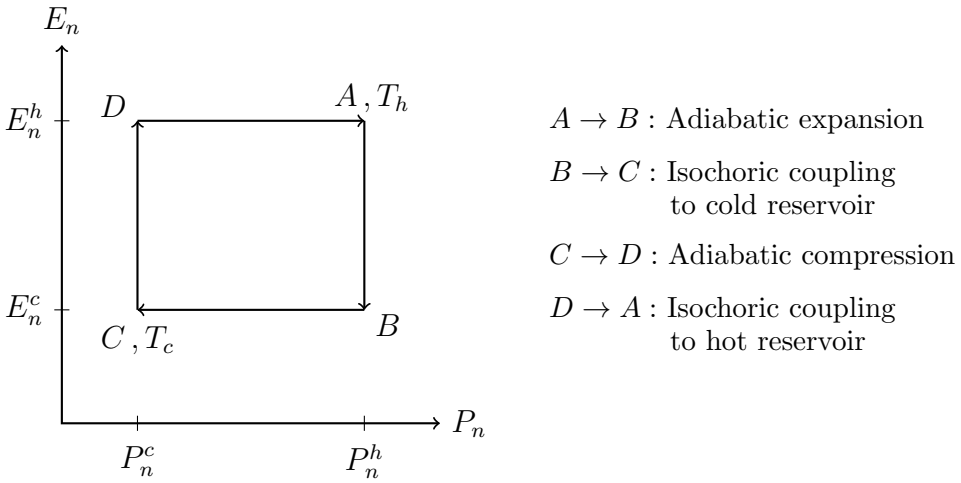

Figure 2.2: The Otto cycle plotted for the nth energy level (assuming this level contributes with positive work output, i.e. that $P_n^h > P_n^c$).

We can obtain general expressions for the the average work performed during the expansion and compression. Using (2.10b), we find that the work performed during the expansion (compression) is

$$W_{\text{exp(comp)}} = -\sum_n \int_{A(C)}^{B(D)} P_n \, dE_n = \sum_n (E_n^{h(c)} - E_n^{c(h)}) P_n^{h(c)} \,. \tag{2.11}$$

By summing up the work from the expansion and the compression we obtain

$$W = \sum_n (E_n^h - E_n^c)(P_n^h - P_n^c) \,, \tag{2.12}$$

which then is the total average work output per cycle, see e.g. [4].

[4]We can also see that work should imply a change in the energy levels by considering the effect of the expansion and compression in the Otto cycle (which are adiabatic so no heat transfer occurs during them). As the expansion and compression change the confinement region of the particles, it means that the trapping potential is changed. As the trapping potential is part of the Hamiltonian, which determines the energy levels, this should indeed affect the energy levels.

Hamiltonians exhibiting scaling property

Let us now restrict ourselves to non-interacting particles, such that the two-body interaction term, v in (2.7), is zero. Different Hamiltonians, for non-interacting particles, are then distinguished from each other by the form of their respective trapping potentials. For certain trapping potentials (e.g. the infinite square well, the harmonic oscillator etc), one can find that the energy levels satisfy

$$\frac{E_n^h}{E_n^c} = \nu^2\,, \quad \text{for all } n, \tag{2.13}$$

for some number $\nu > 1$ [5]. We say that Hamiltonians where (2.13) holds, exhibit a scaling property. Note that ν describes the compression ratio of the Otto engine (valid when operating non-interacting particles).

For Hamiltonians exhibiting the scaling property (2.13), we can greatly simplify the expression for the work output, (2.12). By denoting the average energy as $\langle E^i \rangle = \sum_n E_n^i P_n^i$, we find

$$W = \langle E^c \rangle (1 - \nu^2) + \langle E^h \rangle (1 - \nu^{-2})\,, \tag{2.14}$$

for the average work output per cycle. A clear similarity can be seen between the expression for work using a quantum working medium (2.14) and the corresponding expression for the classical ideal gas particles, (2.3), in the previous section. The two expressions appear analogous by recalling that the average energy for classical, ideal gas particles is $Nk_BT/2$ and with ν corresponding to the compression ratio, V_c/V_h. However, the values of the work output for the classical and quantum particles need not be the same. As the work output for the quantum medium, (2.14), depends on the energy levels, the effects from particle statistics will enter and affect the output.

With Boltzmann distributed occupation-probabilities, it is found that we have to satisfy

$$T_h > \nu^2 T_c\,, \tag{2.15}$$

in order to do positive work. We derive (2.15) in Appendix B, closely following Ref. [3]. Note that (2.15) has the same form as the positive-work condition for the Otto engine operating a classical, ideal gas, (2.4), with ν as the compression ratio.

Excitation energies and excitation-probabilities

To simplify the discussion of the results later on, it is convenient to sometimes talk about the energy levels in terms of their excitation energies from the ground state. We define $\tilde{E}_n^i \equiv E_n^i - E_0^i$ as the excitation energy from the ground state ($n = 0$) to the nth level. We can then rewrite the work output, (2.12), in terms of the excitation energies[5]

$$\begin{aligned} W &= \sum_n ((E_n^h - E_0^h) - (E_n^c - E_0^c))(P_n^h - P_n^c) \\ &= \sum_n (\tilde{E}_n^h - \tilde{E}_n^c)(P_n^h - P_n^c)\,. \end{aligned} \tag{2.16}$$

[5]We can obtain (2.16) since the occupation-probabilities are normalised to unity, such that $\sum_n E_0^i (P_n^h - P_n^c) = E_0^i((\sum_n P_n^h) - (\sum_n P_n^c)) = E_0^i(1-1) = 0$.

Further, we can rewrite the work output into two terms, W_h and W_c, defined as

$$W_i \equiv \sum_n (\tilde{E}_n^h - \tilde{E}_n^c) P_n^i \,, \tag{2.17}$$

with the total work then given by $W = W_h - W_c$. Since W_h only depends on T_h and W_c only on T_c, it will allow us to conveniently discuss the effect of each temperature on the work output. Note that W_h $(-W_c)$ corresponds to the work of the expansion (compression), W_{exp} (W_{comp}) in (2.11), but differing by the constant $-(E_0^h - E_0^c)$. This makes W_h $(-W_c)$ go to zero at $T_h = 0$ $(T_c = 0)$, while W_{exp} (W_{comp}) goes to a constant at zero temperature.

We see that in W_i, the excitation energy difference between the hot and the cold reservoir, $\tilde{E}_n^h - \tilde{E}_n^c$, enter as a factor. When dealing with non-interacting particles, we can use the scaling property $\tilde{E}_n^c = \nu^{-2} \tilde{E}_n^h$. Thus, we can write (2.17), as

$$W_i = (1 - \nu^{-2}) \sum_n \tilde{E}_n^h P_n^i \,. \tag{2.18}$$

The scaling property will therefore allow us to discuss the work output in terms of the excitation energy at the hot reservoir solely, instead of in terms of the excitation energy difference, $\tilde{E}_n^h - \tilde{E}_n^c$.

Finally, we can also write the Boltzmann factors, (2.16), in terms of the excitation energies. We have

$$P_n^i = \frac{\mathrm{e}^{-E_n^i/(k_B T_i)} \, \mathrm{e}^{E_0^i/(k_B T_i)}}{Z_i \, \mathrm{e}^{E_0^i/(k_B T_i)}} = \frac{\mathrm{e}^{-\tilde{E}_n^i/(k_B T_i)}}{\tilde{Z}_i} \,, \tag{2.19}$$

where

$$\tilde{Z}_i = \sum_n \mathrm{e}^{-(E_n^i - E_0^i)/(k_B T_i)} = \sum_n \mathrm{e}^{-\tilde{E}_n^i/(k_B T_i)} \,.$$

Written on the form (2.19), we can see the Boltzmann factors as excitation-probabilities, i.e. the probability for the ground state to be excited to a specific energy level. The Boltzmann factors make excitations to higher energy levels less likely to occur. The temperature, or rather $k_B T_i$, acts like sort of a "cut-off" value, where excitation energies a lot greater than $k_B T_i$, i.e. $\tilde{E}_n^i \gg k_B T_i$, will be heavily suppressed ($P_n^i \sim 0$) and excitation energies much less than $k_B T$, i.e. $\tilde{E}_n^i \ll k_B T_i$, will have considerable occupation-probability ($P_n^i \sim 1/Z_i$), relatively speaking [8].

Chapter 3

Method

In this chapter we will discuss how we can solve the Schrödinger equation numerically and hence obtain the energy levels of our system, so that we are able to calculate the work output in the Otto engine. Calculating the work output involves summing over all energy levels, so in principle we would need to obtain all energy levels of the system. However, as our occupation-probabilities are Boltzmann distributed, the higher energy levels are suppressed and negligible (the temperatures of the heat reservoirs effectively decide at what energy the contributions will be negligible). Nonetheless, we must still obtain a large energy spectrum in general, and it is for this purpose we use the so called configuration interaction method. In this thesis we implement the configuration interaction method using a B-spline basis. We apply the method utilizing the occupation-number representation of many-body quantum mechanics. The occupation-number representation is described in several standard textbooks treating many-particle quantum mechanics, see e.g. Refs. [11], [12] or [13]. In this chapter we will thus treat these concepts, starting with some of the basic theory of many-body quantum mechanics in the occupation-number representation, before discussing the configuration interaction method and B-splines. At the end of this chapter we will discuss the trapping potential and the two-body interaction used for our simulations.

3.1 Many-body quantum systems in the occupation-number representation

3.1.1 Wave function symmetry

In this thesis we will look at particles that are either bosons or fermions. Bosons have symmetric wave functions, while fermions have anti-symmetric wave functions. We illustrate what this means by considering the wave function of an N-particle system, which we denote by $\Psi(x_1, \ldots, x_k, \ldots, x_l, \ldots, x_N)$, where x_k is the coordinate for the kth particle. Next, we define a permutation operator, P_{kl}, which has the effect of interchanging the coordinates of two particles, the kth and the lth in this case. Applied to our wave function, we find

$$P_{kl}\,\Psi(x_1, \ldots, x_k, \ldots, x_l, \ldots, x_N) = \Psi(x_1, \ldots, x_l, \ldots, x_k, \ldots, x_N)\,. \tag{3.1}$$

A symmetric, Ψ_S, and an anti-symmetric, Ψ_A, wave function is then defined as wave functions that the permutation operator has the following effects on

$$\begin{aligned} P_{kl}\,\Psi_S(x_1,\ldots,x_k,\ldots,x_l,\ldots,x_N) &= \Psi_S(x_1,\ldots,x_k,\ldots,x_l,\ldots,x_N) \\ P_{kl}\,\Psi_A(x_1,\ldots,x_k,\ldots,x_l,\ldots,x_N) &= -\Psi_A(x_1,\ldots,x_k,\ldots,x_l,\ldots,x_N) \end{aligned} \quad . \tag{3.2}$$

For a non-interacting N-particle system, the symmetry properties of bosons and fermions decide how they respectively populate the single-particle states of the system. One says that bosons follow Bose-Einstein statistics, while fermions follow Fermi-Dirac statistics. From the anti-symmetry of the wave functions for fermions, it follows that no two fermions can occupy the same single-particle state or the same coordinate, which is known as the Pauli exclusion principle. Considering, on the other hand, a system of N non-interacting identical bosons, their symmetric wave function does not pose any problems having multiple particles occupying the same single-particle state.

Additionally, it is also found that particle statistics and spin go hand in hand. Fermions have half-integer spin while bosons have integer spin. In this thesis, we will only consider spin-polarised particles. This means that the particles will only have one spin state, and therefore we ignore any effects that could occur due to spin. For further details about fermions and bosons, see e.g. Ref. [13].

3.1.2 Occupation-number representation

To build up a complete set of many-particle basis states we use a complete set of single-particle states, $\{|\phi_k\rangle\}$, as the foundation. In the occupation-number representation, we specify how many particles occupy each single-particle state (i.e. specify the occupation-number). We write the many-particle states, sometimes called *Fock* states, on the form $|n_1, n_2, \ldots, n_k, \ldots\rangle$, where n_k denotes the number of particles in the single-particle state k. The specific single-particle occupancies for a many-particle state is referred to as a *configuration*. Note that $|\phi_k\rangle = |0,\ldots,0,1_k,0,\ldots\rangle$, where 1_k means that there is one particle in the kth single-particle state.

Further, we introduce the annihilation and creation operators a_k^- and a_k^+ respectively, which destroy and create one particle in single-particle state k, respectively. The creation and annihilation operators satisfy the algebra

$$\text{Bosons} \begin{cases} [a_k^\pm, a_l^\pm] = 0 \\ [a_k^-, a_l^+] = \delta_{kl} \end{cases}, \quad \text{Fermions} \begin{cases} \{a_k^\pm, a_l^\pm\} = 0 \\ \{a_k^-, a_l^+\} = \delta_{kl} \end{cases}, \tag{3.3}$$

where $[\,,]$ and $\{\,,\}$ are the *commutator* and *anti-commutator*, defined as $[c,b] = cb - bc$ and $\{c,b\} = cb + bc$ for two arbitrary operators c, b. The statistics of the fermions and bosons are incorporated in the commutation and anti-commutation relations, (3.3). The numerical factors when applying the operators on a state consisting of N identical bosons or N identical fermions are

$$\text{Bosons} \begin{cases} a_k^+|n_1,n_2,\ldots,n_k,\ldots\rangle = \sqrt{n_k+1}|n_1,n_2,\ldots,n_k+1,\ldots\rangle \\ a_k^-|n_1,n_2,\ldots,n_k,\ldots\rangle = \sqrt{n_k}|n_1,n_2,\ldots,n_k-1,\ldots\rangle \end{cases}, \tag{3.4}$$

and

$$\text{Fermions} \begin{cases} a_k^+|n_1, n_2, \ldots, 0_k, \ldots\rangle = (-1)^{\sum_{l<k} n_l}|n_1, n_2, \ldots, 1_k, \ldots\rangle \\ a_k^+|n_1, n_2, \ldots, 1_k, \ldots\rangle = 0 \\ a_k^-|n_1, n_2, \ldots, 0_k, \ldots\rangle = 0 \\ a_k^-|n_1, n_2, \ldots, 1_k, \ldots\rangle = (-1)^{\sum_{l<k} n_l}|n_1, n_2, \ldots, 0_k, \ldots\rangle \end{cases} . \tag{3.5}$$

Now we turn to how the Hamiltonian will look using the occupation-number representation. The general Hamiltonian we will be dealing with, where we include a two-body interaction v, is of the form

$$H = \sum_k h(x_k) + \frac{1}{2}\sum_{k\neq l} v(x_k, x_l)\,. \tag{3.6}$$

Above we have introduced an abbreviated form for the one-body operators (the kinetic term and the trapping potential), namely

$$h(x) = -\frac{\hbar^2}{2m}\frac{\partial^2}{\partial x^2} + V(x)\,. \tag{3.7}$$

With this notation, we can write the Hamiltonian in occupation-number representation, as

$$H = \sum_{kl}\langle k|h|l\rangle a_k^+ a_l^- + \frac{1}{2}\sum_{klmn}\langle kl|v|mn\rangle a_k^+ a_l^+ a_n^- a_m^-\,, \tag{3.8}$$

where

$$\langle k|h|l\rangle = \int \phi_k^*(x)h(x)\phi_l(x)\,dx\,, \tag{3.9a}$$

$$\langle kl|v|mn\rangle = \iint \phi_k^*(x)\phi_l^*(x')v(x,x')\phi_m(x)\phi_n(x')\,dx\,dx'\,. \tag{3.9b}$$

Note that in (3.9), $\phi_k(x)$ is the spatial representation of the single-particle states $|\phi_k\rangle$, i.e. $\phi_k(x) = \langle x|\phi_k\rangle$. Further, to obtain the Hamiltonian on the form in (3.8), the single-particle basis $\{|\phi_k\rangle\}$ is assumed to be an orthonormal basis. For the derivation of (3.8), we refer to e.g. Refs. [12] or [13].

3.2 Configuration interaction method

The configuration interaction method we use is not an approximative method in itself, so we can in principle obtain any desired degree of accuracy to our solutions. Let us look at the outline of the method scheme. We want to solve the Schrödinger equation, for a system of N interacting particles, i.e.

$$H|\Psi\rangle = E|\Psi\rangle\,, \tag{3.10}$$

where $|\Psi\rangle$ is an energy eigenstate and E the corresponding energy. Following the previous section, we start by choosing a single-particle basis $\{|\phi_k\rangle\}$, and construct a many-particle basis while utilizing the occupation-number representation. The general form of the Hamiltonian is then given by (3.8). Let us write the many-particle basis states as

$\{|\Phi_\mu\rangle\}$, where a specific μ corresponds to some tuple $\{n_1, n_2, \ldots\}$ describing the occupancies of each single-particle state in the occupation-number representation. Utilising the completeness relation for the many-particle states, we can expand the energy eigenstate $|\Psi\rangle$ in the many-particle basis, i.e.

$$|\Psi\rangle = \sum_\mu c_\mu |\Phi_\mu\rangle \,, \tag{3.11}$$

where $c_\mu = \langle\Phi_\mu|\Psi\rangle$ are the expansion coefficients. Acting with $\langle\Phi_\nu|$ on (3.10), we can write the Schrödinger equation on matrix form in the many-particle basis, as

$$\begin{pmatrix} \langle\Phi_1|H|\Phi_1\rangle & \langle\Phi_1|H|\Phi_2\rangle & \cdots \\ \langle\Phi_2|H|\Phi_1\rangle & \langle\Phi_2|H|\Phi_2\rangle & \cdots \\ \vdots & \vdots & \ddots \end{pmatrix} \begin{pmatrix} c_1 \\ c_2 \\ \vdots \end{pmatrix} = E \begin{pmatrix} c_1 \\ c_2 \\ \vdots \end{pmatrix} . \tag{3.12}$$

The creation and annihilation operators in H determine which matrix elements, $\langle\Phi_\nu|H|\Phi_\mu\rangle$, are non-zero by coupling the many-particle states that affect each other. The values of the matrix elements are then obtained by evaluating the integrals in (3.9). Once the matrix representation for the Hamiltonian is constructed, we can diagonalise it and obtain the eigenvalues, being the energy levels of our system. For the numerical implementation, the diagonalisation was done using the LAPACK library, see [14].

As is seen from the outlined scheme above, the configuration interaction method does not by itself introduce any approximations to the solution. We are instead limited by numerical restrictions. We can in general expect the complete set of single-particle wave functions, $\{|\phi_k\rangle\}$, to be infinite. Consequently, our many-particle states would also constitute an infinite set. We must then introduce a truncation in order to instead deal with a finite set of equations, which we can treat numerically. The truncation will imply that the energy levels obtained from solving the Schrödinger equation necessarily are approximate. By changing the truncation to allow more many-particle states in the calculations, we can find out if our chosen truncation is fine to use, or if it reduces the accuracy of the final results to such an extent that they are no longer valid. If, when we change the truncation, the results are unchanged to an appropriate degree of precision, we can imagine that we have reached a convergent solution. We will see in more detail how the truncation is made when discussing B-splines in the next section.

Since the number of many-particle states grows very rapidly with respect to particle number, the configuration interaction method is limited to few-particle systems, $N \lesssim 5$, depending on the specific problem. The reason why the growing number of many-particle states is a problem is because it increases the size of the Hamiltonian, which we both need to construct and diagonalise. We thus see that the configuration interaction method might not be suitable for arbitrary purposes. However, if we require a large and accurate energy spectrum, it is a useful method if we allow ourselves to be restricted to low particle numbers.

3.3 B-splines

The library for the configuration interaction method used in this thesis has been implemented using a basis built up of B-splines [15], which are piecewise polynomials. The

jth B-splines of order p, $B_{j,p}(x)$, can be specified through the recurrence relation (see Ref. [16])

$$B_{j,p}(x) = \frac{x - t_j}{t_{j+p-1} - t_j} B_{j,p-1}(x) + \frac{t_{j+p} - x}{t_{j+p} - t_{j+1}} B_{j+1,p-1}(x) \,, \tag{3.13}$$

for $p \geq 2$. The B-splines of order 1, are given by

$$B_{j,1}(x) = \begin{cases} 1 \,, & t_j < x < t_{j+1} \\ 0 \,, & \text{otherwise} \end{cases} \,. \tag{3.14}$$

Above, t_j are called knot points, and consist of a non-decreasing sequence of numbers $t_{j+1} \geq t_j$. Each B-spline, $B_{j,p}(x)$, is only non-zero between t_j and t_{j+p}.

We can see from (3.13), that increasing the order by 1, the polynomial degree of the B-splines increase by 1. The order thus determines the polynomial degree of the B-splines, and we see that B-splines of order p have a polynomial degree of order $p-1$. In Fig. 3.1, we sketch the general features of how the B-splines would look. Additionally, note that the knot points need not be distributed equidistant over the region under consideration, but could be concentrated at convenient positions in order to improve numerical precision at regions where it might be necessary.

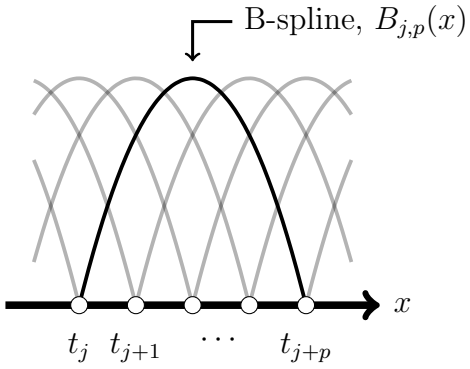

Figure 3.1: Sketch of a B-spline set-up. One B-spline is highlighted (black) while the others are faded (light-grey) for clarity. The knot points, t_j, are shown as circles on the x-axis.

The B-spline basis set will not in general be an orthonormal basis when constructed. However, we can instead construct an orthonormal basis from the B-spline set. A convenient choice is to take the orthonormal basis states, $|\phi\rangle$, to be the single-particle eigenstates of the one-body term of the Hamiltonian, i.e. h given by (3.7). We then have

$$h|\phi\rangle = \epsilon|\phi\rangle \,, \tag{3.15}$$

where ϵ is the single-particle energy corresponding to $|\phi\rangle$. Let us denote the jth B-splines, for a fixed order, in ket-space by $\{|B_j\rangle\}$, such that $B_j(x) = \langle x|B_j\rangle$, where we have omitted the subscript for the order as we keep it fixed (we will also keep the order fixed later in our numerical calculations). We can express the single-particle eigenstates in the B-spline basis as

$$|\phi\rangle = \sum_j d_j |B_j\rangle \,, \tag{3.16}$$

where d_j are the expansion coefficients. Substituting (3.16) into (3.15) and acting with $\langle B_{j'}|$, we can write (3.15) on matrix form as

$$\begin{pmatrix} \langle B_1|h|B_1\rangle & \langle B_1|h|B_2\rangle & \cdots \\ \langle B_2|h|B_1\rangle & \langle B_2|h|B_2\rangle & \cdots \\ \vdots & \vdots & \ddots \end{pmatrix} \begin{pmatrix} d_1 \\ d_2 \\ \vdots \end{pmatrix} = \epsilon \begin{pmatrix} \langle B_1|B_1\rangle & \langle B_1|B_2\rangle & \cdots \\ \langle B_2|B_1\rangle & \langle B_2|B_2\rangle & \cdots \\ \vdots & \vdots & \ddots \end{pmatrix} \begin{pmatrix} d_1 \\ d_2 \\ \vdots \end{pmatrix} . \tag{3.17}$$

The matrix elements in (3.17) are given by

$$\langle B_{j'}|h|B_j\rangle = \int B^*_{j'}(x)h(x)B_j(x)\,dx\,, \tag{3.18a}$$

$$\langle B_{j'}|B_j\rangle = \int B^*_{j'}(x)B_j(x)\,dx\,. \tag{3.18b}$$

Thus, by solving (3.17) we obtain the orthonormal basis states $|\phi\rangle$, and can from there proceed with the configuration interaction method as described in the previous section.

The B-spline basis size is specified directly through the B-spline order and the number of knot points, by the relation (Number of B-splines = Number of Knot Points + B-spline order − 4). We thus see that this directly effects the size and accuracy of the single-particle basis states, as the single-particle basis states are obtained by solving (3.17). In this sense we see how we effectively introduce a truncation in our system. If we run our simulation for a certain number of B-splines and compare it to the result of another run with an increased (or decreased) number of B-splines, we imagine the solution is converged if the results for the two runs are sufficiently close. We discuss the convergence checks further in Appendix A.

3.4 System set-up

When we start to analyse the Otto engine we will first look at the non-interacting case, so that we examine the simplest cases and observe the underlying physics. Next, we will extend the system, such that the particles interact with each other by a two-body interaction. In this section we therefore give some general details regarding the systems we will consider and discuss the interaction we will use.

3.4.1 Single-particle energy levels and compression ratio

The trapping potential, $V(x)$, that we will consider in this thesis is the infinite square well potential. We use this potential because of its simple form, which is

$$V(x) = \begin{cases} 0\,, & 0 < x < L \\ \infty\,, & \text{otherwise} \end{cases}\,, \tag{3.19}$$

where L is the well length. The single-particle system in an infinite square well is described in most standard textbooks, see e.g. [7], [11], where the energy levels (and corresponding wave functions) are analytically known. The single-particle energy levels are given by

$$\epsilon_k = \frac{\hbar^2\pi^2(k+1)^2}{2mL^2} = (k+1)^2\epsilon_0\,, \qquad k = 0, 1, 2, \ldots\,. \tag{3.20}$$

For a system undergoing the Otto cycle, the well length is the parameter restricting the spatial distribution of the particles and hence is the parameter varied during the expansion and compression. We can then realise that the compression ratio for the infinite square well is given by

$$\nu = \frac{L_c}{L_h}\,, \tag{3.21}$$

where L_i describes the well length at the hot and the cold reservoir for $i = h$ and $i = c$ respectively.[1]

3.4.2 Two-body interaction

The two-body interaction we consider in this thesis is of the form

$$v(x_k, x_l) = g\,\frac{\hbar^2}{mL_h^2}\,\mathrm{erfcx}\!\left(\frac{|x_k - x_l|}{2b}\right), \tag{3.22}$$

where g is an interaction strength, b a parameter we will keep fixed (discussed more below) and $\mathrm{erfcx}(x)$ is the exponentially scaled error function, $\mathrm{erfcx}(x) = \exp(x^2)\,\mathrm{erfc}(x)$, with $\mathrm{erfc}(x)$ being the complementary error function, $\mathrm{erfc}(x) = 2\pi^{-1/2}\int_x^\infty \exp(-t^2)\,dt$. The full Hamiltonian can then be written as

$$H = \frac{\hbar^2}{mL_h^2}\left[\sum_k\left(-\frac{1}{2}\frac{\partial^2}{\partial X_k^2} + V(L_h X_k)\right) + \frac{g}{2}\sum_{k\neq l}\mathrm{erfcx}\!\left(\frac{|X_k - X_l|}{2(b/L_h)}\right)\right], \tag{3.23}$$

where we have introduced the dimensionless position coordinates

$$X_k = \frac{x_k}{L_h}\,.$$

Effective 1D Coulomb interaction

The reason we use the two-body interaction (3.22), is because it is an effective 1D Coulomb interaction for a 3D system under a cylindrical confinement that is strong enough for the system to be frozen in the ground state of the cylindrical confinement, see Ref. [17]. The cylindrical confinement is taken to be in the yz-plane, which we will call the transverse direction; and it would be realised by a 2D isotropic harmonic oscillator, for which the oscillator frequency will be denoted by $\omega_\perp$. In the x-direction, or the longitudinal direction, we will have the system we have set-up before, i.e. using the infinite square well as the trapping potential. The full Hamiltonian is then

$$\begin{aligned} H = &\sum_k\left(-\frac{\hbar^2}{2m}\frac{\partial^2}{\partial x_k^2} + V(x_k)\right) \\ &+ \sum_k\left(-\frac{\hbar^2}{2m}\left(\frac{\partial^2}{\partial y_k^2} + \frac{\partial^2}{\partial z_k^2}\right) + \frac{m\omega_\perp^2}{2}(y_k^2 + z_k^2)\right) + \frac{1}{2}\sum_{k\neq l}\frac{q^2}{\kappa|\mathbf{r}_k - \mathbf{r}_l|}\,. \end{aligned} \tag{3.24}$$

[1] We can also find $\nu = L_c/L_h$ by using the scaling property (2.13) on the single-particle energy levels (3.20).

where the last term is the Coulomb interaction, with q as the charge of the particles, $\kappa = 4\pi\epsilon_r\epsilon_0$ the background permittivity, (ϵ_r being the relative permittivity and ϵ_0 the vacuum permittivity ($\epsilon_0 \approx 8.855 \cdot 10^{-12}$ Fm^{-1})), and $\mathbf{r}_k = (x_k, y_k, z_k)$.

Let us now assume that the cylindrical confinement is really strong. If it is sufficiently strong, the energy contribution from the Coulomb interaction is very low relative to the energy needed to excite the transverse oscillator, for which we require $\hbar\omega_\perp$. We could then take the system to be in the ground state of the transverse direction, such that the wave function for the system, $\Psi(\mathbf{r}_1, \dots \mathbf{r}_N)$, could be approximated to

$$\Psi(\mathbf{r}_1, \dots \mathbf{r}_N) = \Phi(x_1, \dots, x_N)\psi(y_1, z_1) \cdots \psi(y_N, z_N)\,. \tag{3.25}$$

Here, $\Phi(x_1, \dots, x_N)$ is the wave function in the longitudinal direction and $\psi(y, z)$ is the wave function in the transverse direction, being the single-particle ground state wave function for a 2D harmonic oscillator, i.e.

$$\psi(y, z) = \frac{1}{(2\pi b^2)^{1/2}} \exp\left(-\frac{y^2 + z^2}{4b^2}\right). \tag{3.26}$$

In (3.26), b is the *oscillator length* of the ground state, i.e. the square root of the mean square displacement of a particle in the ground state of a harmonic oscillator, and given by

$$b = \sqrt{\frac{\hbar}{2m\omega_\perp}}\,. \tag{3.27}$$

With the transverse direction fixed in its ground state, we can integrate out the transverse degrees of freedom, and study the longitudinal direction in an effective 1D problem. The derivation of reducing the Coulomb interaction to (3.22) is done in Appendix D, where we follow the derivation done in Ref. [18]. Furthermore, the interaction strength g can then be identified as

$$g = \frac{mL_h}{\hbar^2}\frac{\sqrt{\pi}q^2}{2\kappa(b/L_h)}\,. \tag{3.28}$$

The space the system operates in would look like Fig. 3.2, which we could realise in e.g. a nanowire. The system would then be confined to operate in the longitudinal direction of the wire. Additionally, the oscillator length b could be seen as a measurement of the radius of wire

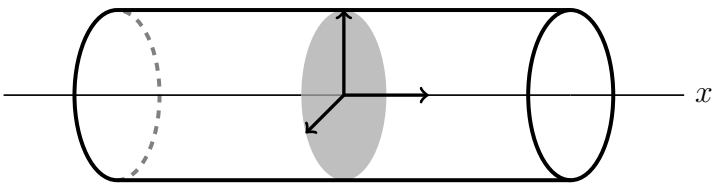

Figure 3.2: Sketch of the system under a strong cylindrical confinement. The system will effectively be confined to the x-dimension, being the longitudinal direction of the wire.

Note again that we can only identify (3.22) as an effective 1D Coulomb interaction in case the cylindrical confinement is sufficiently strong. When our system undergoes the Otto cycle, the increased thermal energy from coupling to the heat reservoirs could possibly

excite the transverse system from its ground state, which we will discuss further below how to avoid. Moreover, a large enough interaction strength, g, would mean that the energy contribution from the Coulomb interaction to the transverse direction is no longer negligible, and hence give rise to some amount of excitations. To increase the transverse confinement strength, we would increase $\omega_\perp$. As we see in (3.27), $\omega_\perp$ is related to the inverse square of b, i.e., we have

$$\omega_\perp = \frac{\hbar}{2mb^2}\,. \tag{3.29}$$

We would therefore increase the transverse confinement strength by decreasing b. If the results we obtained do not change much when decreasing b, we could imagine that it indicates that the transverse confinement is sufficiently strong for the approximation (3.25) to hold, and hence for the interaction (3.22) to be identified with the effective 1D Coulomb interaction. We discuss this further in Appendix C, in relation to some of the results obtained in Ch. 5. The main conclusion is that we would require further investigation in order to be sure whether we could actually say that (3.22) can be identified as an effective 1D Coulomb interaction in our case. However, it seems possible that it is the case for fermions, while for bosons it seems less likely.

Temperature restriction on b

In order to at least minimise the probability to excite the transverse system due to thermal energy, we can restrict the value of b such that the excitation-probability, up to some temperature, becomes small. The excitation energy to the first excited state of the transverse oscillator (being 2D and isotropic) is given by $\hbar\omega_\perp$. With our system following a Boltzmann distribution, this means that we require $k_BT \ll \hbar\omega_\perp$. Using (3.27), we find that this means

$$b^2 \ll \frac{\hbar^2}{2mk_BT}\,. \tag{3.30}$$

As we will consider the infinite square well, we can write (3.30) in terms of the single-particle ground state energy level of the infinite square well, divided by k_B, i.e. ϵ_0^h/k_B. We obtain

$$\left(\frac{b}{L_h}\right)^2 \ll \frac{1}{\pi^2 T(\epsilon_0^h/k_B)^{-1}}\,.$$

If we then were to realise our system in a nanowire, (b/L_h) would measure the ratio of the wire's radius to its length (the length when the system is coupled to the hot reservoir). To remain in the quantum regime, we focus on lower temperature values, such that $T \lesssim 100\epsilon_0^h/k_B$. With this limit, we find $(b/L_h) \ll 0.03$. Experimentally, real nanowires can be constructed with the possibility for the length to radius ratio reaching 1000 or more, i.e. corresponding to $(b/L_h) \sim 0.001$, see e.g. [19]. We will take $(b/L_h) = 0.005$ and use that value henceforth.

3.4.3 Parity

The number of equations to numerically solve when finding the eigenvalues for a $D \times D$ is proportional to D^3 [20].[2] When diagonalising our Hamiltonian matrix, the computa-

[2]We used the LAPACK routine F08GAF (DSPEV), see Ref. [20], when diagonalising the Hamiltonian matrix.

tion time will therefore grow rapidly as the size of the many-body basis, given by D, is increased. However, the computation time can be significantly reduced by using the concept of parity. Parity is an operator that inverts the spatial coordinates, such that $\mathbf{r} = (x, y, z) \to (-x, -y, -z) = -\mathbf{r}$. The eigenvalues of the parity operator can be shown to be ± 1. Thus, if a state is an eigenfunction of parity, it implies that its wave function, $\Psi(\mathbf{r})$, is an odd or even function, $\Psi(-\mathbf{r}) = \pm\Psi(\mathbf{r})$. One says that the state is odd or even under parity [11].

As our Hamiltonian, (3.23), is an even function of the spatial coordinates, it is invariant under parity. The Hamiltonian therefore commutes with the parity operator, and common eigenstates for the two exist [11]. We can thus split up our states in odd and even parity states, allowing us to solve the Schrödinger equation for the odd and even parity states separately, since the Hamiltonian will not couple the odd and the even parity states. With the infinite square well as the trapping potential, the number of even and odd states will approximately be the same in the numerical calculations, such that we have around $D/2$ odd and $D/2$ even states. This effectively reduces the Hamiltonian matrix to two $D/2 \times D/2$ matrices, implying that the computation time to diagonalise it will be proportional to $2\,(D/2)^3 = D^3/4$. We can thus reduce the computation time for the diagonalisation by roughly a factor of four, which makes an important difference for long calculations.

Chapter 4

Non-interacting particles

4.1 Set-up specifics

In this and the next chapter, we will present and discuss the results for the Otto engine using a working medium of non-interacting respectively interacting particles in the infinite square well. The energy levels for non-interacting particles in the infinite square well are known analytically, so we do not require to solve the Schrödinger equation numerically in this case. When dealing with interacting particles, we do have to solve the Schrödinger equation numerically. In this case we apply the configuration interaction method, as described in the previous chapter.

Let us repeat the details about the systems we are going to consider:

- We will be looking at few-particle systems, $N \leq 4$, consisting of either fermions or bosons.
- The particles we treat will be spin-polarised, meaning that spin will not be a relevant factor in our considerations. Thus, for $N = 1$, bosons and fermions will be equivalent, so the results are the same for the two in the single-particle case.
- When the system has been coupled to the hot (cold) reservoir, it is Boltzmann distributed and maintains the same occupation-probabilities throughout the expansion (compression) stroke, since the driving is done adiabatically.

Throughout this chapter we will use the index 0 to refer to the ground state energy. Thus, the many-particle ground state will be denoted E_0 and the single-particle ground state $\epsilon_0 = \hbar^2\pi^2/(2mL^2)$.

4.2 Work output dependence on particle type

We start by comparing the work output of non-interacting fermions and bosons for fixed compression ratio $L_c/L_h = 2$ and specific N. In Fig. 4.1 the ratio of work output of fermions to bosons, W_F/W_B, is plotted against the temperature of the hot, T_h, and the cold, T_c, reservoirs, for $N = 3$. The plot shows, qualitatively, whether fermions have a larger work output than bosons, i.e. if $W_F/W_B > 1$, or if bosons have a larger work output than fermions, $W_F/W_B < 1$. Speaking in broad terms, it seems that fermions have

a larger work output than bosons at "higher" temperatures; i.e. increasing T_h or both T_h and T_c we will,[1] at some point, have that fermions produce more work than bosons. In the same way, bosons have a larger work output at "lower" temperatures, i.e for low values of T_h and T_c.

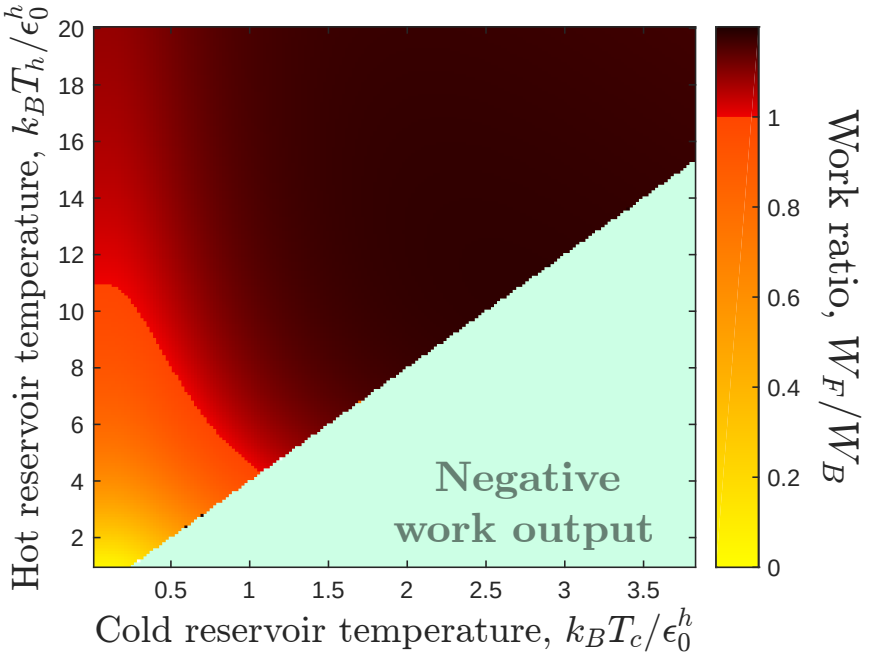

Figure 4.1: *Non-interacting particles.* The figure shows the work output ratio of three fermions to three bosons, W_F/W_B, plotted against T_h and T_c (in units of ϵ_0^h/k_B). The compression ratio is fixed to $L_c/L_h = 2$. The border $W_F/W_B = 1$ is made more distinct by having a strong color shift between $W_F/W_B < 1$ and $W_F/W_B > 1$, in order to emphasize where fermions respectively bosons have greater work output. Light-green is used to indicate the negative work output region, i.e. the region where both the systems of fermions and bosons have negative work output (both systems have work done to them).

We can understand the behaviour seen in Fig. 4.1 by looking at the properties of the single-particle energy levels. The sketch in Fig. 4.2 shows the lowest single-particle energy levels in the infinite square well with well length L. The sketch compares how a system of three non-interacting fermions respectively three non-interacting bosons would populate the single-particle energy levels in their respective many-particle ground states. The Pauli principle restricts to one fermion in each single-particle energy level (as we are dealing with spin-polarised particles), so that they populate the lowest three single-particle levels. The bosons, on the other hand, all populate the single-particle ground state.

[1] As long as T_c is not increased such that the ratio T_h/T_c becomes lower than $\nu^2 = (L_c/L_h)^2$.

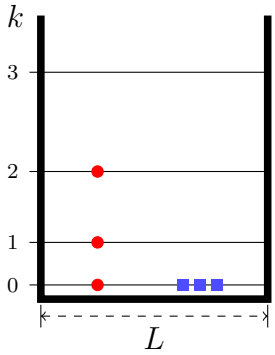

Figure 4.2: *Non-interacting particles.* Sketch of the single-particle energy levels of the infinite square well potential (denoted by k and shown as thin horizontal lines), as populated by three fermions (red circles) or three bosons (blue squares) in their respective many-particle ground states. The well length is denoted L.

Let us look at the excitation energy from the many-particle ground state to the first excited state for the situation in Fig. 4.2. We see that the first excited many-particle state for the three non-interacting fermions is to move the fermion in the 3rd single-particle level to the 4th. The excitation energy would then be $(4^2 - 3^2)\epsilon_0 = 7\epsilon_0$. For the three non-interacting bosons, on the other hand, the excitation energy would only be $(2^2 - 1^2)\epsilon_0 = 3\epsilon_0$, moving one of the bosons in the 1st single-particle level to the 2nd single-particle level. In general, the excitation energy to a specific level for a many-particle system is higher when dealing with fermions than with bosons, i.e. $\tilde{E}_{n,\mathrm{Ferm}} > \tilde{E}_{n,\mathrm{Bos}}$. This follows from combining two observations:

(i) The single-particle energy levels, ϵ_k, go as k^2 in the infinite square well, such that the single-particle energy level spacings are monotonically increasing.[2]

(ii) The Pauli principle will restrict the configuration options for fermions, such that bosons will have more configurations involving the lower single-particle levels.

In Fig. 4.3, we plot the lowest many-particle energy levels against their excitation energies, for three fermions and for three bosons. We see that the higher excitation energies for the fermions give them a sparser energy spectrum.

[2]The level spacing go as $\epsilon_{k+1} - \epsilon_k \sim (k+1)^2 - k^2 \sim k$, and thus grow larger and larger as higher levels are considered.

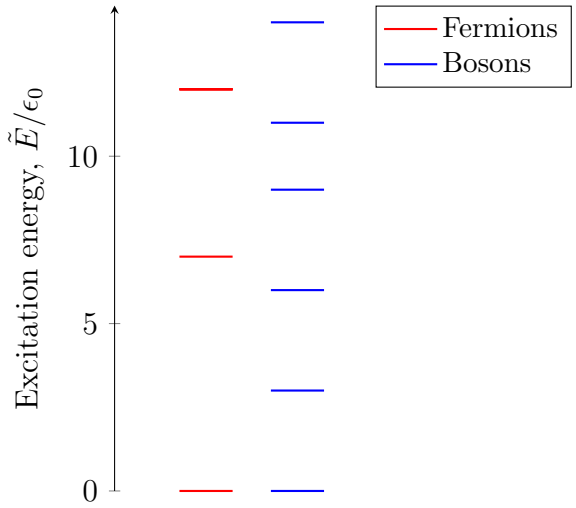

Figure 4.3: *Non-interacting particles.* The energy levels of three fermions and three bosons respectively, with the energy measured in terms of the excitation energy, $\tilde{E} = E - E_0$ (in units of $\epsilon_0 = \hbar^2\pi^2/(2mL^2)$).

When the systems undergo the Otto cycle, we mentioned earlier (Sect. 2.2) that the work output could be written as $W = W_h - W_c$. We had defined W_i, $i = h, c$, by

$$W_i = (1 - \nu^{-2}) \sum_n \tilde{E}_n^h P_n^i \,, \tag{4.1}$$

where $\nu = L_c/L_h$ is the compression ratio and the temperature dependence of W_h (W_c) is only on T_h (T_c). We can argue that a low enough temperature T_h (T_c), will result in W_h (W_c) being larger for bosons than for fermions. This would follow since the excitation energy to the first excited state is lower for bosons. We can thus imagine that for a low enough temperature T_h (T_c), the bosons will be able to have non-negligible excitations to their first excited state, while the fermions will essentially be frozen in their ground state. Thus, we have $W_{h,\text{Bos}} > 0$ ($W_{c,\text{Bos}} > 0$), and $W_{h,\text{Ferm}} \approx 0$ ($W_{c,\text{Ferm}} \approx 0$).

We note that as the energy spectrum for fermions is sparser than for bosons (see Fig. 4.3), the excitation-probability for the highest, non-negligible excitation will be higher for fermions than for bosons. This follows since the excitation-probabilities have to add up to unity, and as the fermions have less states than the bosons that have to split the probabilities. Thus, as T_h (T_c) is increased and the fermions start to be able to have non-negligible excitations to their first excited state, we could expect that it will contribute a larger factor in W_h (W_c). It therefore seems reasonable that as T_h (T_c) reaches some value, W_h (W_c) will become larger for the fermions than for the bosons.

If we now consider the total work output, $W = W_h - W_c$, at very low values for T_c, we would essentially have $W_c \approx 0$ such that $W = W_h$. We then expect bosons to have a larger work output at lower values of T_h, while fermions have a larger work output as T_h is increased over some value. This is just what we see in Fig. 4.1, when looking at $T_c \approx 0$.

When letting T_c increase to non-zero values, there will be a non-negligible work cost due to W_c. Let us increase T_c from zero by keeping T_h fixed, such that W_h = constant. As T_c starts to become high enough to excite the system, we expect W_c to be larger for

bosons than for fermions (due to the bosons lower excitation energy). We therefore find $W_{\text{Ferm}} = W_{h,\text{Ferm}} - W_{c,\text{Ferm}} = W_{h,\text{Bos}} - W_{c,\text{Ferm}} > W_{h,\text{Bos}} - W_{c,\text{Bos}} = W_{\text{Bos}}$, i.e. as T_c becomes high enough to have an effect on the system, it decreases the total work output for the bosons more than for the fermions. We can see this in Fig. 4.1 by that the border $W_F/W_B = 1$ bends downwards as we increase T_c.

The temperature dependence of fermions and bosons we have observed, has been described before in Ref. [5]. They considered a fixed T_c (with a value "...cold enough to see the combined effect of both energy level spacings and particle statistics") and found that for lower values of T_h, bosons had a larger work output than fermions, while for higher values instead fermions had a larger work output. They also argued that the reason is a combination of the particle statistics and the specific trapping potential considered (for the infinite square well it is the monotonically increasing energy level spacings that is the significant feature).

4.3 Work output dependence on particle number

How would fermions and bosons compare if we were to change the particle number? We can expect the qualitative behaviour to be the same as for $N = 3$ in the previous section. This follows from that no matter what N we consider, the monotonically increasing (single-particle) energy level spacings in the infinite square well, together with the Pauli principle for the fermions, will make the fermions have higher excitation energies and a sparser energy spectrum than the bosons. One difference we can note is in the actual values of the excitation energies. Let us look at the excitation energy to the first excited many-particle state as an example. For bosons the excitation energy to the first excited many-particle state requires the same amount of energy for any N, since the many-particle ground state for bosons consists of all particles in the single-particle ground state. For the fermions, however, we need to move the particle occupying the highest single-particle level, and it will occupy a higher level for a larger N. Because the single-particle energy level spacings in the infinite square well are monotonically increasing, the excitation energy for the first excited state will therefore be higher as N is increased.

The result of the increased excitation energy to the first excited state for the fermions (while the bosons' is unchanged) when increasing the particle number, is that the fermions will require higher temperatures in order to start producing more work than the bosons. In Figs. 4.4a and 4.4b, we see the work ratio W_F/W_B plotted for $N = 2$ and $N = 4$, respectively. We see that the qualitative behaviour for the two N cases is indeed similar with the $N = 3$ case in Fig. 4.1. However, we do see that the region where $W_F/W_B < 1$ is expanded when going from $N = 2$ to $N = 4$, as we expected it to be. This agrees with what was found in Ref. [5], where one can see that when N is increased, it requires a higher value of T_h (using a fixed T_c) for fermions to get a larger work output than bosons.

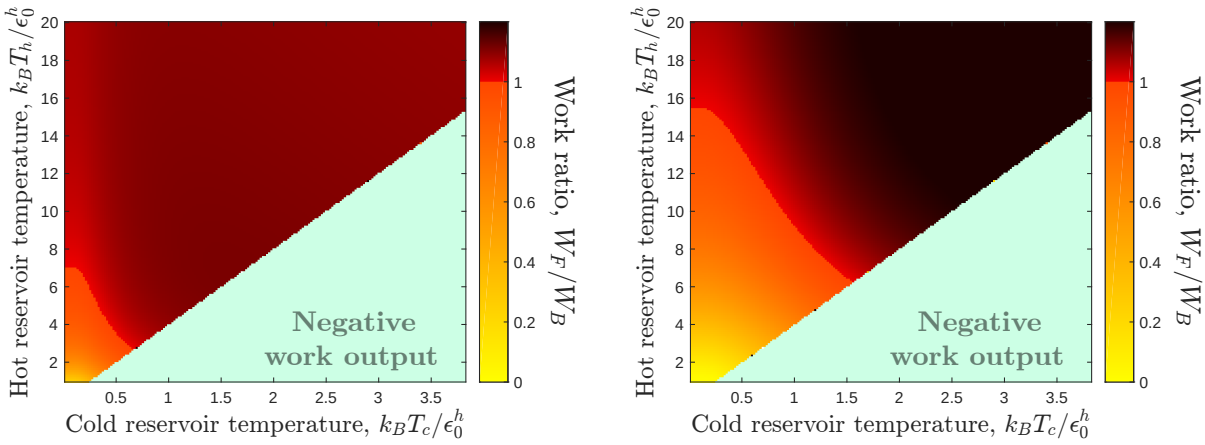

(a) $N = 2$ **(b)** $N = 4$

Figure 4.4: *Non-interacting particles.* The figures show the work output ratio of fermions to bosons, W_F/W_B, plotted against T_h and T_c (in units of ϵ_0^h/k_B). The compression ratio is fixed to $L_c/L_h = 2$. The border $W_F/W_B = 1$ is made more distinct by having a strong color shift between $W_F/W_B < 1$ and $W_F/W_B > 1$, in order to emphasize where fermions respectively bosons have greater work output. Light-green is used to indicate the negative work output region.

There are other differences in the work output of an Otto engine that we can observe when changing the particle number, which we see if we examine fermions and bosons separately. For example, we could ask ourselves "which number of particles produce the largest work output depending on the temperatures of the hot and the cold reservoirs, T_h and T_c?"

First, let us consider how fermions of different particle number would compare to each other. As noted above, the excitation energy to the first excited many-particle state will increase as N is increased. But we can realise that all excitation energies must increase, since the increased N would mean that we have additional particles we have to populate (and therefore contribute to higher energy). We see this also in Fig. 4.5a, where we plot the lowest energy levels against their excitation energies for two and four fermions. We thus have that a larger N have higher excitation energies and a sparser energy spectrum than a smaller N. This is, qualitatively, how we above found that the energy spectra for fermions and bosons compared (see e.g. Fig. 4.3). We could then imagine that, considering the work output, we should qualitatively have similar behaviour when looking at "fermions with smaller N versus fermions with larger N" as when looking at "bosons versus fermions".

If we turn to discuss bosons of different N, we see in Fig. 4.5b that the lowest excitation energies for the bosons are the same for $N = 2$ and $N = 4$. We actually have that all excitation energies for $N = 2$ also occur for $N = 4$. This follows from that for bosons, the many-particle ground state consists of all particles occupying the single-particle ground state. Thus, for all ways we can excite the $N = 2$ case, we could also excite the $N = 4$ case by keeping two of the bosons in the single-particle ground state. As we could also move around the two bosons we kept in the single-particle ground state, we obtain additional excitation energies for $N = 4$ as well.

It is a bit difficult to draw any expectations from the bosons' energy spectra. As the lower excitations are the same for bosonic systems, it is not directly clear how the weight of the

expectation-probabilities affect the work output.

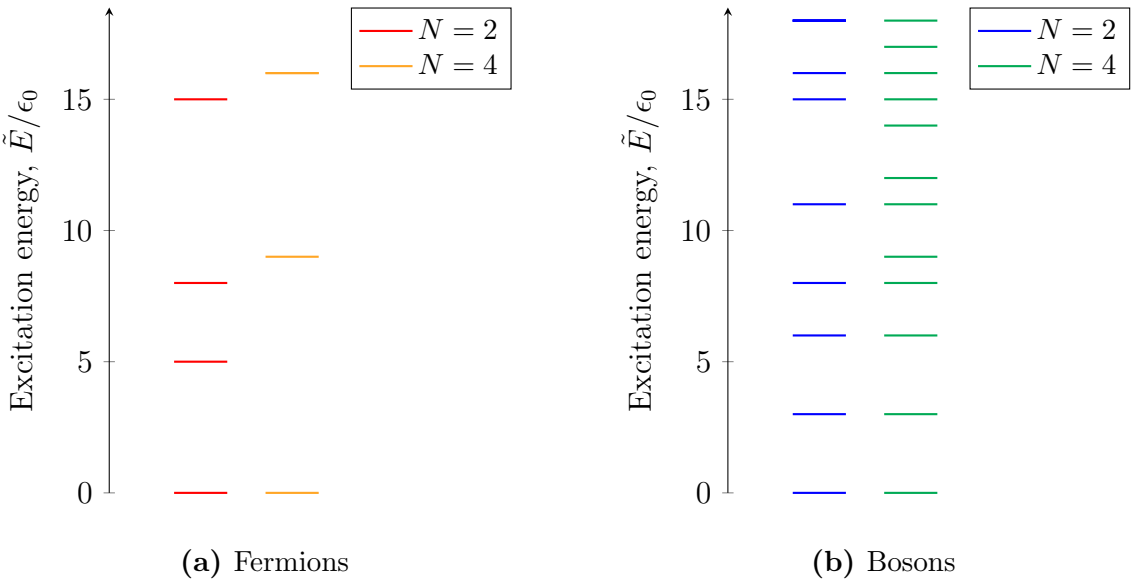

(a) Fermions **(b)** Bosons

Figure 4.5: *Non-interacting particles.* The energy levels using $N = 2$ and 4 for (a) fermions and (b) bosons. The energy is measured in terms of the excitation energy, $E - E_0$ (in units of $\epsilon_0 = \hbar^2\pi^2/(2mL^2)$).

In Fig. 4.6, for given temperatures T_h and T_c, we look at the work output for systems with $N = 1, 2, 3, 4$ and display whichever has the largest work output. Thus, we plot which N-particle Otto engine has the largest work output, W; considering $N = 1, 2, 3, 4$ and a compression ratio of $L_c/L_h = 2$. Fermions are considered in Fig. 4.6a, which behave as we expected. We see that the lower N has largest work output for the lower temperatures (i.e. low T_h and low T_c). Also, the transition between different N being the top producer looks similar to the transition between $W_F/W_B < 1$ and $W_F/W_B > 1$ when comparing fermions and bosons (see Fig. 4.1 or 4.4).

In Fig. 4.6b we consider bosons. We see that $N = 4$ has the largest work output for any temperatures T_h and T_c, in stark contrast with the result for fermions. It looks like for bosons, increasing the particle number increases the work output. Note, however, that as we do not see how much the work output differ between the different N, it could be that as N is increased, the increase in work output is reduced. We would then reach a point where increasing N will not further increase the work output to any significant degree.

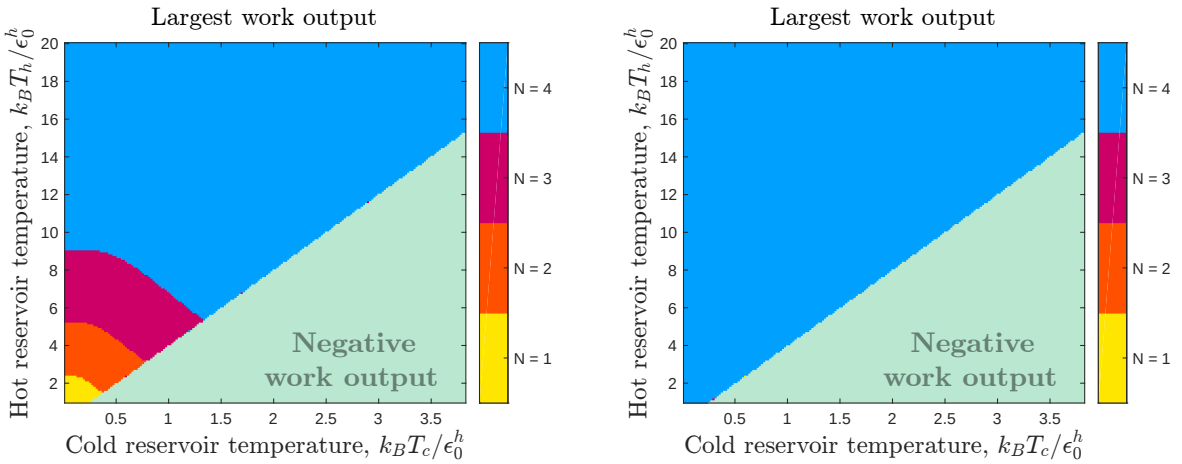

(a) Fermions **(b)** Bosons

Figure 4.6: *Non-interacting particles.* The plots show which N-particle Otto engine has the largest work output, for $N = 1, 2, 3, 4$, depending on the temperatures of the reservoirs, T_h and T_c. The compression ratio is fixed to $L_c/L_h = 2$. Light-green is used to indicate the negative work output region.

We can also look at which N-particle Otto engine has the largest work output *per particle*, W/N. This is plotted in Fig. 4.7, considering $N = 1, 2, 3, 4$ and a compression ratio of $L_c/L_h = 2$. For fermions, Fig. 4.7a, we see that the result is qualitatively similar to Fig. 4.6a, but that the regions for where each N is favourable has been expanded. This could just follow from that when considering work output per particle, the output is decreased more for higher N, shifting the temperature regions where each is favourable to higher values. In Fig. 4.6b, we look at bosons. We see that $N = 1$ has largest work output per particle at any temperatures T_h and T_c. Hence, for bosons, the work output per particle could be thought to decrease as the particle number is increased.

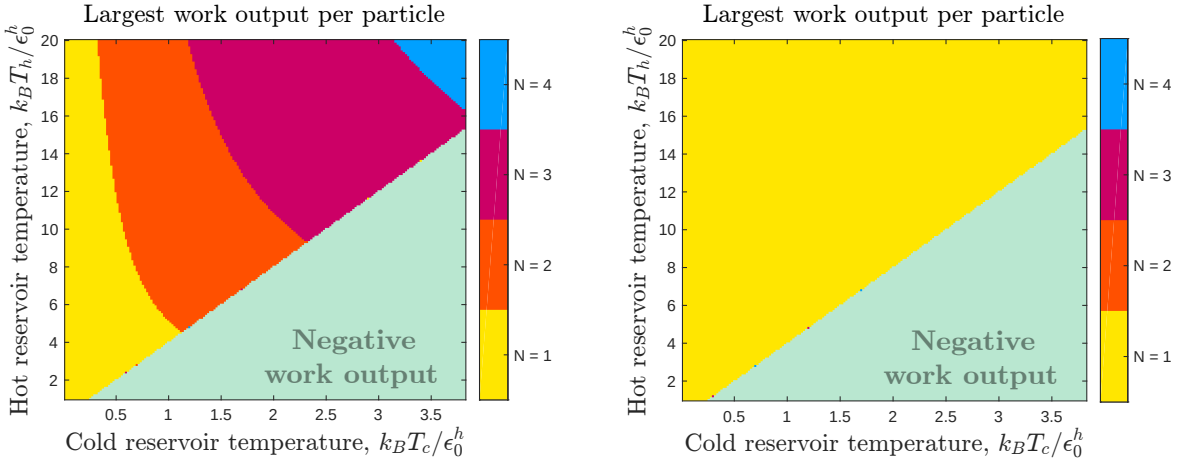

(a) Fermions **(b)** Bosons

Figure 4.7: *Non-interacting particles.* The plots show which N-particle Otto engine has the largest work output per particle, for $N = 1, 2, 3, 4$, depending on the temperatures of the reservoirs, T_h and T_c. The compression ratio is fixed to $L_c/L_h = 2$. Light-green is used to indicate the negative work output region.

4.4 Comparsion to classical ideal gas for different compression ratios

We will finish the examination of the non-interacting particles by looking at how the work output per particle changes as the compression ratio is varied. We will at the same time compare the work output per particle to that of a classical, mono-atomic ideal gas, for which the work output is given by (2.3). As the work output for the classical particles is linear in N, the work output per particle is the same for any N.

In Fig. 4.8, the work output per particle is plotted against the compression ratio for $N = 1, 2, 3, 4$. We consider fermions and bosons separately, with each plot considering different temperatures but with the same temperature ratio $T_h/T_c = 16$. As discussed at the end of Sect. 2.1, this means that the classical work output (per particle) is maximized for the compression ratio $L_c/L_h = (T_h/T_c)^{1/4} = 2$, which we will denote ν_{CL}.

Let us denote the compression ratio corresponding to maximum work output by ν_{max}, and see how it differs for particle type, particle number, and temperature. The general behaviour seems to be that at low temperatures (Figs. 4.8a and 4.8b), $\nu_{\text{max}} > \nu_{\text{CL}}$ for both fermions and bosons. Moreover, we see that for fermions, ν_{max} is higher when N is increased, while for bosons, ν_{max} seems to be more or less the same for all N. Increasing the temperatures makes $\nu_{\text{max}} \to \nu_{\text{CL}}$. Sufficiently high temperatures make all N considered, for both fermions and bosons, have $\nu_{\text{max}} = \nu_{\text{CL}}$, which we can see in Figs. 4.8e and 4.8f.

A possible explanation to the behaviour of ν_{max} could be argued from looking at the excitation energies of the fermions and bosons. As we mentioned earlier and saw in Fig. 4.5b, the excitation energies of a system with a smaller number of bosons are also the excitation energies of a system with a greater number of bosons. This could then be a reason to why the bosons seem to have maximum work output at the same compression ratio. The fermions, on the other hand, do not share excitation energies in the same way, which could make different N have maximum work output at different compression ratios. That all N, for both fermions and bosons, tend to have a maximum work output at ν_{CL} as the temperatures are increased, could be thought of an indication that the systems tend to the classical one in the high temperature limit. As the temperatures are increasing, we will have more and more accessible excitations. At some point, it will effectively be a continuum, and we could expect the quantum particles to behave like the classical ones. If we look a the plots we can also see that when we increase the temperature T_h from $2\epsilon_0^h$ to $16\epsilon_0^h$ and finally to $64\epsilon_0^h$ (with $T_c = 0.125\epsilon_0^h$, ϵ_0^h and $4\epsilon_0^h$ respectively), the curves in each plot appears to become closer together, for both fermions and bosons. This indicates that the quantum cases approach each other and the classical case, as the temperature is increased.

Another observation that can be made from Fig. 4.8 is how the work output of the classical ideal gas compares to the fermions and the bosons. For sufficiently low temperatures, e.g. the temperatures considered in Figs. 4.8a and 4.8b, we see that the classical ideal gas is capable of producing more work than the fermions and the bosons. However, if we increase the temperatures this changes. For the fermions, increasing the temperature enough, as in Fig. 4.8e, the classical engine has lower work output than all of the N-

fermion engines, at all compression ratios considered. For the bosons though, it seems that having higher temperatures, Figs. 4.8d and 4.8f, only makes $N = 1$ and 2 being able to have larger work output than the classical case.

The reason that the classical particles can have larger work output at very low temperatures could be an effect of that the classical particles have a continuous energy spectrum. At the low temperatures in Figs. 4.8a and 4.8b, both fermions and bosons will not have any substantial amount of excitations. This will leave them essential frozen in their ground states, such that very little to no work is produced. The classical case, however, is not limited by needing temperatures high enough for any excitations to be probable, as the energy spectrum is continuous. This could then lead to the larger work output for the classical particles at the very low temperatures. But, when increasing the temperatures, the occupation-probabilities, being Boltzmann factors, will give the quantum particles a relatively large weight to the accessible excitations in the work output. Hence, the work output of the quantum particles might become higher than the classical ones. We see that this could be the case for the fermions, however for the bosons only $N = 1, 2$ get a higher work output than the classical case. This explanation is therefore, at best, only partially applicable. We could speculate that, since the energy spectrum for the bosons become denser as N is increased, and the energies for a lower N appear as a subset of the energies for a higher N (see Fig. 4.5b), the probabilities does not give a large enough weight to shift the work output in favour to the bosons, compared to the classical particles, for the higher N. But this would need further investigation to assess.

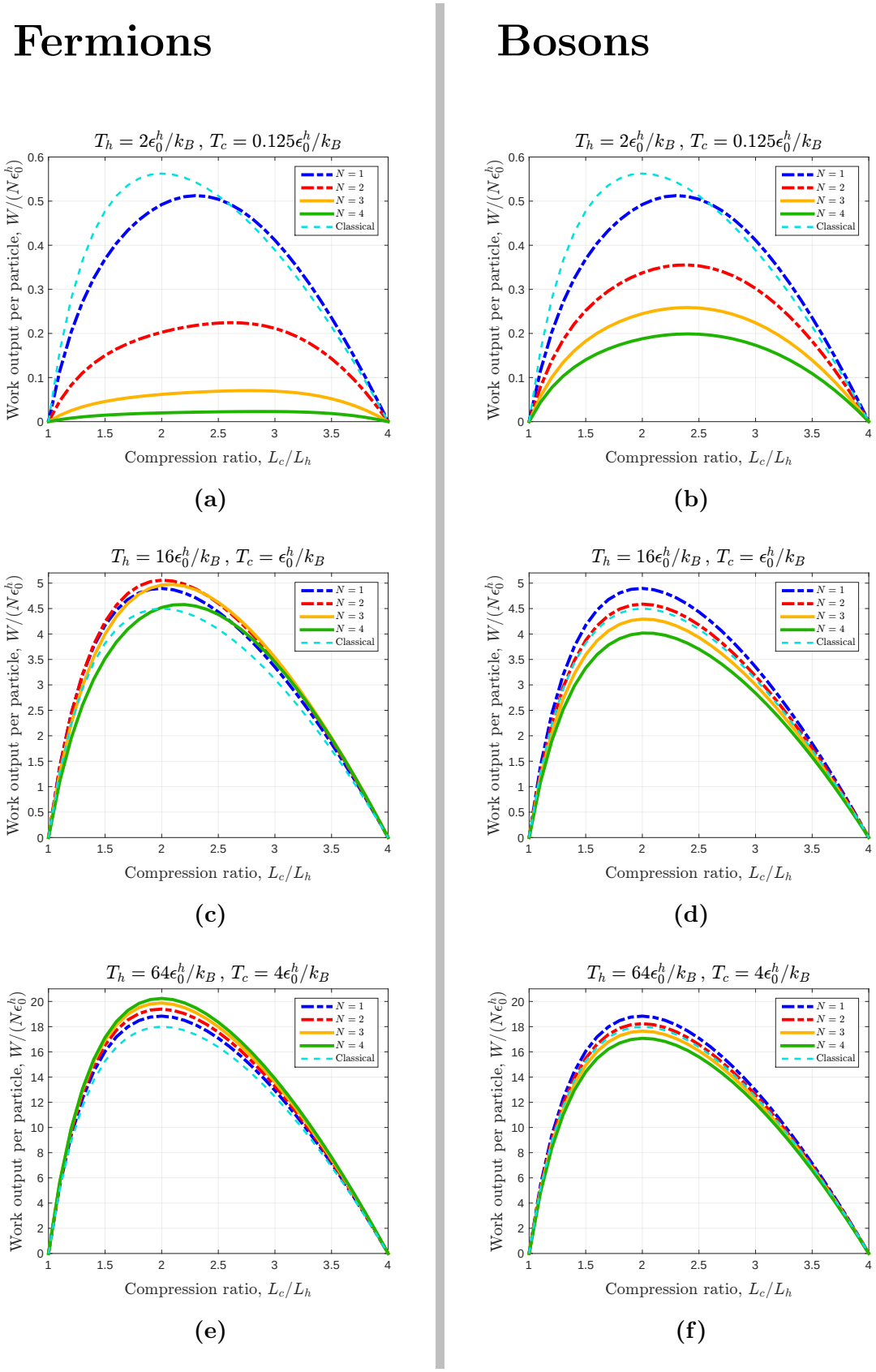

Figure 4.8: *Non-interacting particles.* The figures show the work output per particle, W/N, for different N-particle Otto engines, versus the compression ratio L_c/L_h. The temperature ratio T_h/T_c is kept fixed at $T_h/T_c = 16$ for all figures, while the temperatures T_h and T_c are varied. The left-hand side plots consider fermions, while the right-hand side plots consider bosons.

4.5 Conclusion

We have seen that non-interacting fermions and bosons behave considerably different when undergoing the Otto cycle. The choice of trapping potential[3] combined with the particle statistics of the fermions and bosons could be seen as the root to their difference in work output. We summarize the results and comment on the physical significance below.

- When comparing Otto engines of fermions and bosons with the same particle number, it seemed that, in general, fermions produce more work at "higher" temperatures (T_h high or T_h and T_c high), while bosons produced more work at "lower" temperatures (T_h and T_c low). This had also been found in Ref. [5], where they for a fixed T_c, saw that low T_h made bosons have a larger work output, while increasing T_h high enough made fermions have a larger work output. As higher temperatures will lead to a larger total work output for any system (since the heat input from the temperature of the hot reservoir is what we use to transform to work), we can imagine that if we want to optimize a hypothetical, experimental engine, fermions (e.g. electrons) could be preferable to use over bosons.

- We found that for fermions, the number of particles yielding the largest work output and the largest work output per particle, depended on the temperatures of the reservoirs. For the bosons, we saw that adding more particles resulted in a larger work output; while a lower number of particles increased the work output per particle. When constructing an engine, one consideration could then be whether to use a few engines with a larger number of particles in each, or many engines with a few particles in each. As there might be other physical or experimental restrictions as to what case could be realised in an experimental setting, some interesting optimization criterion might be found here.

- Finally, we compared quantum particles to classical (mono-atomic and ideal) particles. We saw that when using fermions, we could have Otto engines with higher work output than ones using the corresponding classical cases. This would indicate us to further study small-scaled Otto engines operating quantum particles, in the hopes that one could possibly use several small engines running quantum particles to compete with classical engines (here, of course, a lot more study is needed to investigate finite-time engines).

[3]The main point being that since we used the infinite square well, the single-particle energy level spacings were monotonically increasing.

Chapter 5

Interacting particles

In this chapter we will treat the Otto engine with a working medium of particles that interact through the two-body interaction given by (3.22), i.e.

$$v(x_i, x_j) = g\,\frac{\hbar^2}{mL_h^2}\,\mathrm{erfcx}\left(\frac{|x_i - x_j|}{2b}\right).$$

As we discussed earlier, this could be seen as an effective 1D Coulomb interaction in the limit that the system had a strong cylindrical confinement in its transverse direction. In Appendix C, we look whether we can interpret the interaction as an effective 1D Coulomb interaction for our results. We find that more investigation would be necessary in order to establish if we can. However, it looks possible for the fermions, while not very possible for the bosons.

Throughout this chapter we will keep the parameter b fixed, using $b = 0.005L_h$ (as we discussed in Sect. 3.4.2). The number of B-splines used for the systems in the different figures are given in Appendix A, where we also briefly discuss how we checked for convergence of the results in the figures, with respect to the basis sizes used.

5.1 Interaction strength and excitation energies

To understand what effect the interaction will have, let us look at how the excitation energies for the lowest many-particle levels change as the interaction strength, g, is varied, see Fig. 5.1. The figure looks at a system with three fermions and three bosons, with a well length L. Starting to increase the interaction strength from zero to non-zero values, the excitation energies increase for both fermions and bosons. We can however note that the increase is greater for the bosons. We can argue that it follows as a consequence from that the fermions obey the Pauli principle.

The Pauli principle restricts fermions from getting into contact with each other. Hence, the interaction will not affect fermions for the very close inter-particle distances. Bosons will, on the other hand, be affected by the interaction at very close inter-particle distances. Thus, for "weaker" interaction strengths, adding the two-body interaction will not effect the fermions to the same extent as the bosons. However, increasing the interaction strength to higher values, we can expect the interaction to become strong enough so that also bosons cannot get into close contact with each other. At this point the fermions and bosons should essentially behave the same, and the energy levels of the bosons should

have increased in value to become the same as the fermions' levels. In Fig. 5.1 we see that this is the case, where the plotted energy levels of the bosons and the fermions tend to the same value at sufficiently strong interaction strength (happening around $g \sim (15-20)L/b$ for the energy levels in the figure).

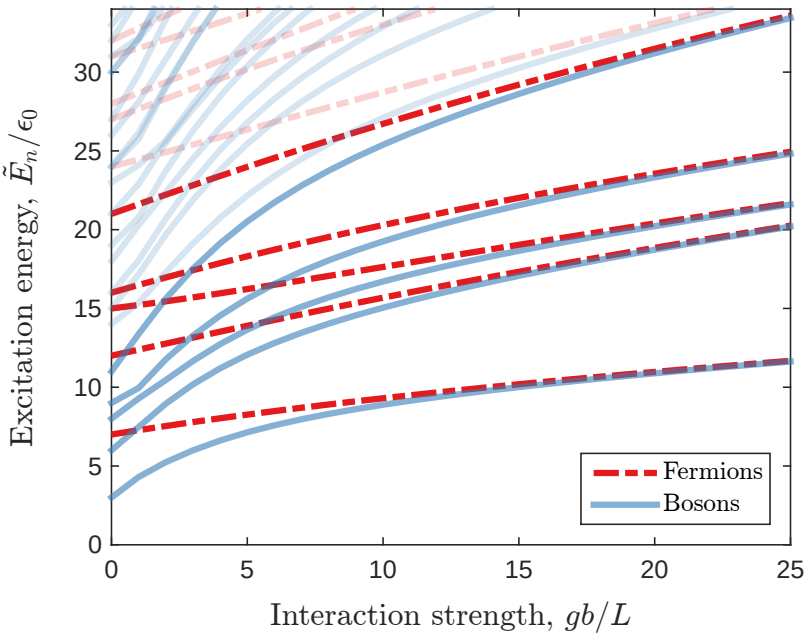

Figure 5.1: *Interacting particles.* Excitation energy to the nth many-particle energy level versus the interaction strength, g. The plot considers three fermions and three bosons. The lines for the 6th and higher excitation states are faded to make the plot more clear.

As the increase in the excitation energies for the bosons are relatively larger than for the fermions, we would expect the bosons to have a more noticeable change in their work output when the interaction is introduced. Further, with increased excitation energies for the interacting fermions and bosons, we predict that the work output would decrease, compared to the non-interacting case, if we consider low enough temperatures T_h and T_c. The reason would be that the excitation-probabilities will become more suppressed, and we would need higher temperatures to obtain non-negligible excitations to the first excited states. However, we could then also expect the work output to increase, for high enough value of T_h, as then the higher excitations will obtain a larger excitation-probability.[1]

In Figs. 5.2a and 5.2b, the work output for three fermions and bosons, respectively, are plotted against the interaction strength, g. The figure considers a compression ratio

[1]Here we neglect the fact that it is the difference between the energies before and after the expansion that enters in the work output, not just the excitation energies (which we discuss more in detail below). For this reason, we could in principle have that the interacting case has larger excitation energies but lower difference between the energies before and after the expansion, such that the interacting case does not actually get a larger work output than the non-interacting case, at high T_h. However, unless the excitation energies for the interacting case have a very strong dependence on the well length, we could expect the difference between the energies before and after the expansion to also increase for the interacting case.

$L_c/L_h = 2$ and uses a fixed temperature ratio, $T_h/T_c = 16$, for all the curves. We can indeed notice that for the lower temperatures, $T_h = 4\epsilon_0^h/k_B$ and $8\epsilon_0^h/k_B$ (with $T_c = 0.25\epsilon_0^h/k_B$ and $0.5\epsilon_0^h/k_B$), the work output decreases when the interaction strength is increased.[2] And for the higher temperatures $T_h = 32\epsilon_0^h/k_B$ and $64\epsilon_0^h/k_B$ (with $T_c = 2\epsilon_0^h/k_B$ and $4\epsilon_0^h/k_B$), the work output increases as g is increased. We also note that for these higher temperature curves, we can clearly see that the work output is increased relatively more for the bosons than for the fermions, as g starts to get non-zero values.

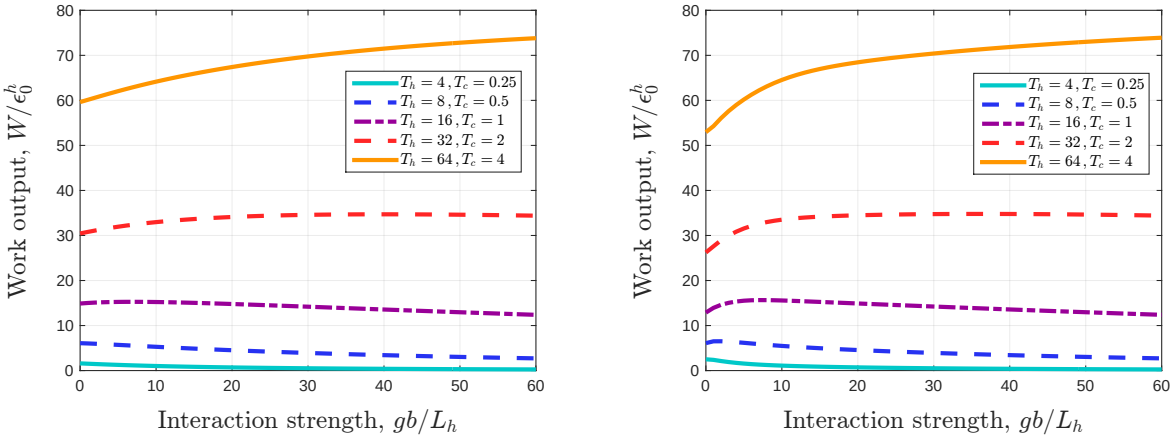

(a) Fermions **(b)** Bosons

Figure 5.2: *Interacting particles.* The plots show the work output dependence on the interaction strength, g. Each figure considers $N = 3$ with fixed compression ratio, $L_c/L_h = 2$. All temperatures are given in units of ϵ_0^h/k_B, and all curves have the same temperature ratio $T_h/T_c = 16$.

To be able to discuss how fermions and bosons compare to each other in some more detail, we should examine how the excitation energies change as the well length is expanded; since the difference between the energies before and after the expansion, $\tilde{E}_n^h - \tilde{E}_n^c$, enters the expression for the work output.[3]

In Fig. 5.3a, we plot the ratio of the excitation energy for fermions to bosons, $\tilde{E}_{1,\text{Ferm}}/\tilde{E}_{1,\text{Bos}}$, as a function of the well length, L, in units of a reference value L'. Note that the plot only considers the excitation energy to the first excited state, however, higher excitations showed a similar behaviour. The figure considers $N = 3$ and $g = 2.5L'/b$ (with $b = 0.005L'$). We see that the excitation energies for the fermions and bosons become closer in value (the ratio decreases) as the compression ratio is increased. This can be

[2]For the bosons with $T_h = 8\epsilon_0^h/k_B$ and $T_c = 0.5\epsilon_0^h/k_B$, we do see that at the very lowest values of g the work output increases, but then decreases as g is increased further. The reason could be that, for these temperatures, slightly increased excitation energies still have sufficient excitation-probability to increase the work output. But as the energies are increased further when g is increased, the excitation-probabilities become more suppressed, which instead leads to a decrease in the work output.

[3]Recall that for the non-interacting case, we could use the scaling property of the excitation energies and write $\tilde{E}_n^h - \tilde{E}_n^c = \tilde{E}_n^h(1 - \nu^{-2})$. Thus, as we knew that $\tilde{E}_{n,\text{Ferm}} > \tilde{E}_{n,\text{Bos}}$, it directly followed that $\tilde{E}_{n,\text{Ferm}}^h - \tilde{E}_{n,\text{Ferm}}^c > \tilde{E}_{n,\text{Bos}}^h - \tilde{E}_{n,\text{Bos}}^c$. For the interacting case we do not longer have the scaling property for our excitation energies and hence need to look at how the excitation energies change as the well length is expanded.

explained from that the non-interacting part of our Hamiltonian go as $1/L^2$ (since we use the infinite square well), while the interacting part of our Hamiltonian go as $\sim 1/L$ (as it can be an effective Coulomb interaction). When the well length is increased, the interaction part will therefore have a relatively larger contribution to the energy, compared to the non-interacting part. Consequently, the behaviour of the fermions and the bosons will more and more be dominated by the interaction part, meaning that they will become more and more similar to each other.

As a complement, Fig. 5.3b shows the relative difference between $\tilde{E}_1^c/\tilde{E}_1^h$ and[4] $(L_c/L_h)^{-2}$, where $(L_c/L_h)^{-2}$ was the value of $\tilde{E}_n^c/\tilde{E}_n^h$ for non-interacting particles. Since the relative difference (for both fermions and bosons) become larger as the compression ratio is increased, it indicates that the contribution from the interaction to the energy indeed becomes more significant as the well length is expanded.

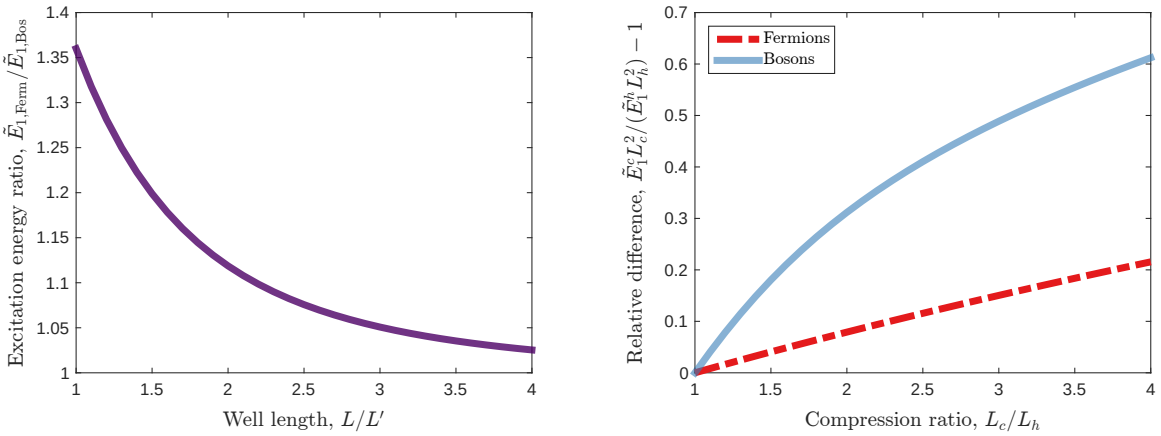

(a) **(b)**

Figure 5.3: *Interacting particles.* (a) Ratio of the excitation energies of the first excited states for fermions to bosons $\tilde{E}_{1,\mathrm{Ferm}}/\tilde{E}_{1,\mathrm{Bos}}$, versus the well length L (in units of some reference length L'). (b) Relative difference between $\tilde{E}_1^c/\tilde{E}_1^h$ and $(L_c/L_h)^{-2}$, i.e. $\tilde{E}_1^c L_c^2/(\tilde{E}_1^h L_h^2) - 1$; for fermions (red dash-dotted line) and bosons (solid light-blue line) plotted against the compression ratio L_c/L_h. Both plots consider three fermions and three bosons, with an interaction strength $g = 2.5L'/b$ in (a) and $g = 2.5L_h/b$ in (b) (with $b = 0.005L'$ and $b = 0.005L_h$, respectively).

5.2 Work output dependence on particle type

Let us recall expression (2.17), i.e.

$$W_i = \sum_n (\tilde{E}_n^h - \tilde{E}_n^c) P_n^i \,,$$

where $i = h, c$ and the total work is given by $W = W_h - W_c$. From the discussion in the previous section, we found that $\tilde{E}_{n,\mathrm{Ferm}}/\tilde{E}_{n,\mathrm{Bos}}$ decreased as the well length was increased.

[4]Again, the higher excitations showed qualitatively similar behaviour as the $n = 1$ case displayed here.

This directly leads to

$$\frac{\tilde{E}^c_{n,\mathrm{Bos}}}{\tilde{E}^h_{n,\mathrm{Bos}}} > \frac{\tilde{E}^c_{n,\mathrm{Ferm}}}{\tilde{E}^h_{n,\mathrm{Ferm}}} \;\Rightarrow\; 1 - \frac{\tilde{E}^c_{n,\mathrm{Ferm}}}{\tilde{E}^h_{n,\mathrm{Ferm}}} > 1 - \frac{\tilde{E}^c_{n,\mathrm{Bos}}}{\tilde{E}^h_{n,\mathrm{Bos}}}\,.$$

If we then use that $\tilde{E}_{n,\mathrm{Ferm}} > \tilde{E}_{n,\mathrm{Bos}}$, we find that $\tilde{E}^h_n(1 - \tilde{E}^c_n/\tilde{E}^h_n) = \tilde{E}^h_n - \tilde{E}^c_n$ is larger for fermions than for bosons. This is qualitatively similar to what we had in the non-interacting case, so we could initially expect that the general features are similar for the interacting case. By this we mean that bosons would have a larger work output at lower values of T_h and T_c, while fermions will have a larger work output at higher values of T_h and T_c.

In Fig. 5.4 we look at the work ratio, W_F/W_B, considering $N = 3$ with a compression ratio of $L_c/L_h = 2$ (i.e. similar set-up as in Fig. 4.1, which is the corresponding plot for the non-interacting case). An effective interaction strength, $g = L_h/b$, is used. We see that at least the left part of the plot, for $T_c \lesssim \epsilon^h_0/k_B$, looks qualitatively similar to the non-interacting case. Let us consider $T_c \approx 0$, such that $W_c \approx 0$ and $W = W_h$. The lower excitation energies for the bosons would mean that they have non-negligible excitations at a lower value of T_h and hence their work output should be larger for low T_h. As T_h is increased, the fermions will begin to have some excitations. As the fermions have fewer non-negligible, excited states, they will get a larger relative weight from the excitation-probabilities. Further, since $\tilde{E}^h_n - \tilde{E}^c_n$ was larger for fermions than bosons, they should contribute to a larger value in W_h. At some T_h, the fermions could therefore be thought to get a larger work output than the bosons (just as in the non-interacting case). This is also what we see, for the very lowest values of T_c, in Fig. 5.4.

If we keep T_h fixed, such that W_h is constant, and increase T_c to values where it starts to make W_c non-negligible, we would find that $W_{c,\mathrm{Bos}} > W_{c,\mathrm{Ferm}}$, again just as for the non-interacting case. However, as the excitation energies for fermions and bosons are relatively closer in the interacting case, we could expect that the difference between $W_{c,\mathrm{Bos}}$ and $W_{c,\mathrm{Ferm}}$ is not as big as in the non-interacting case. This would then mean that the border $W_F/W_B = 1$ should bend off downwards with a less steep slope compared to the non-interacting case. We can see in Fig. 5.4 (and comparing with Fig. 4.1), that this is the case for $T_c \lesssim \epsilon^h_0/k_B$. However, as we increase T_c further, the border $W_F/W_B = 1$ turns upwards. Hence, for the interacting case, in contrast to the non-interacting case, we have $W_F/W_B < 1$ for higher values of T_h and T_c, as long as T_c is large enough compared to T_h.

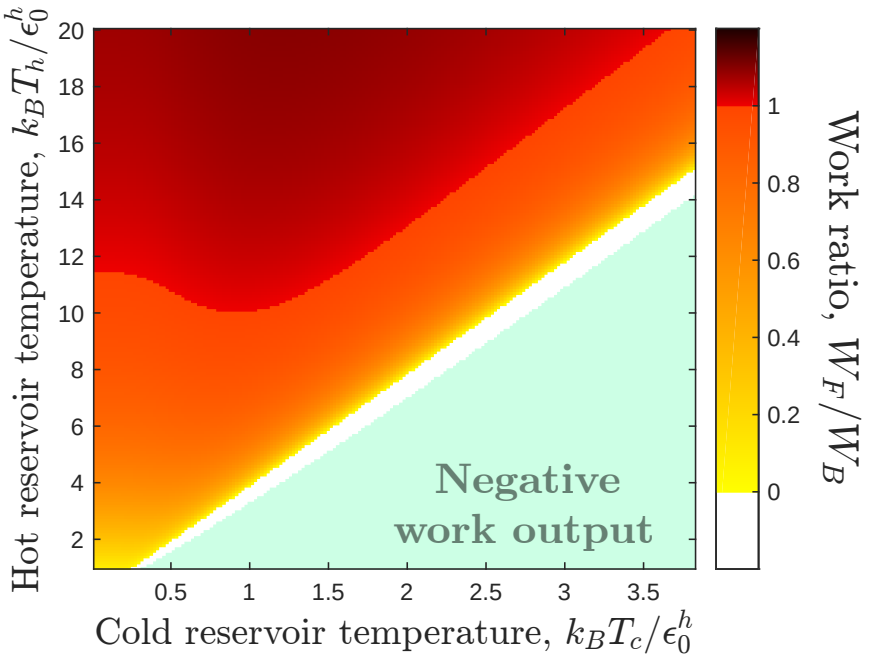

Figure 5.4: *Interacting particles.* The figure shows the work output ratio of three fermions to three bosons, W_F/W_B, plotted against T_h and T_c (in units of ϵ_0^h/k_B). The effective interaction strength is set to $g = L_h/b$, and the compression ratio is fixed to $L_c/L_h = 2$. The border $W_F/W_B = 1$ is made more distinct by having a strong color shift between $W_F/W_B < 1$ and $W_F/W_B > 1$, in order to emphasize where fermions respectively bosons have greater work output. Light-green is used to indicate the negative work output region, i.e. the region where both the systems of fermions and bosons have negative work output (both systems have work done to them).

In Fig. 5.4, we can also see that just above the negative work output region (where both fermions and bosons have negative work output), there is a white line indicating that either the fermions or the bosons have negative work output while the other has positive work output. This suggests that the positive work condition is not the same for fermions and bosons, which it was in the non-interacting case, namely $T_h > (L_c/L_h)^2 T_c$. In Fig. 5.5a, we plot the work output for three fermions and three bosons for fixed T_h over a range of values for T_c, using a compression ratio of $L_c/L_h = 2$. We can clearly see that we do not have the same positive work output condition for the fermions and the bosons. The bosons appear to have a lower bound, able to have positive work output for lower temperature ratios, T_h/T_c, than the fermions. Also note that Fig. 5.5a shows that both the fermions and the bosons can have a positive work output at a lower bound than $T_h > (L_c/L_h)^2 T_c = 4T_c$.

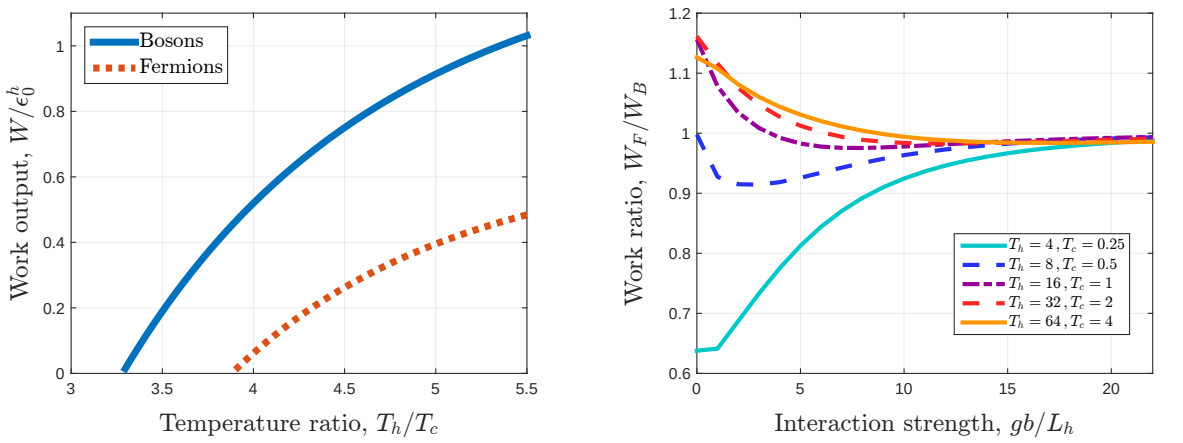

(a) Positive work output

(b) Work ratio versus interaction strength

Figure 5.5: *Interacting particles.* (a) Work output for three fermions and three bosons, plotted against T_h/T_c with fixed $T_h = 3\epsilon_0/k_B$. The interaction strength is set to $g = L_h/b$. (b) The plot show the work output ratio, W_F/W_B, for $N = 3$, as a function of the interaction strength, g. All temperatures are given in units of ϵ_0^h/k_B, and all curves have the same temperature ratio $T_h/T_c = 16$. Both plots consider a compression ratio of $L_c/L_h = 2$.

Finally, as increasing the interaction strength brings the excitation energies of the fermions and the bosons closer together, we expect the work ratio, W_F/W_B, between the two to become closer to unity as g is increased. We visualise this in Fig. 5.5b, where we plot the work ratio for the curves considered in Figs. 5.2a and 5.2b. We see that independent of the values of T_h and T_c considered, the work ratio tends to unity as the interaction strength becomes large enough, as expected.

5.3 Work output dependence on particle number

Let us look a bit into how the work output depends on particle number. First, we will consider how the work ratio between fermions and bosons, W_F/W_B, differs as the particle number is changed. We would expect the qualitative behaviour to be the same for different N. However, as the values of the excitation energies change for different N, the temperature values where $W_F/W_B = 1$ should also change (just as in the non-interacting case). In Fig. 5.6 we look at the work ratio for $N = 2$ and 4. We use a compression ratio of $L_c/L_h = 2$ and an interaction strength, $g = L_h/b$. The plots do show that $N = 2$ and 4 have qualitatively similar behaviour, as has $N = 3$ in Fig. 5.4. One thing to note is that the region for where the bosons have positive work output but the fermions have negative (white line above the negative work output region) is increased in size as N is increased.

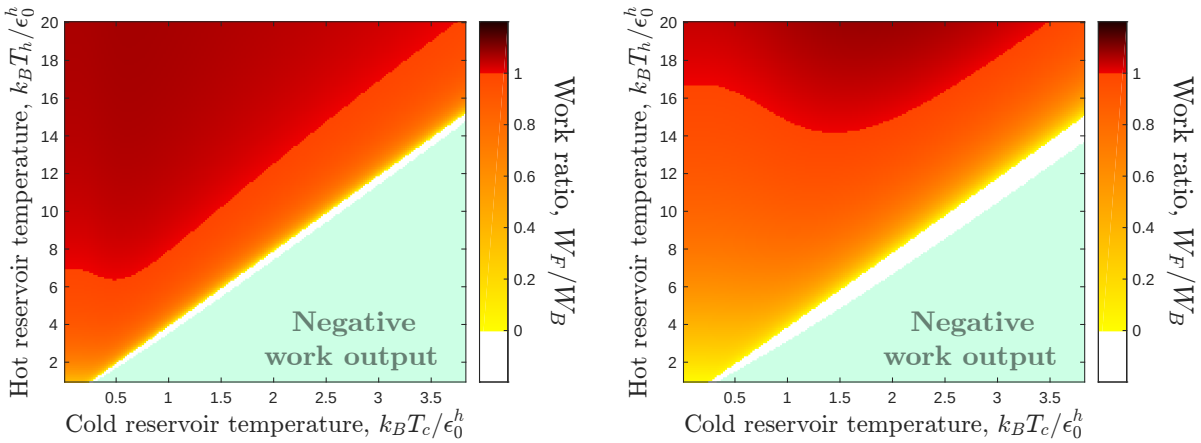

(a) $N = 2$ **(b)** $N = 4$

Figure 5.6: *Interacting particles.* The plots show the work output ratio of fermions to bosons, W_F/W_B, plotted against T_h and T_c (in units of ϵ_0^h/k_B). The effective interaction strength is set to $g = L_h/b$, and the compression ratio is fixed to $L_c/L_h = 2$. The border $W_F/W_B = 1$ is made more distinct by having a strong color shift between $W_F/W_B < 1$ and $W_F/W_B > 1$, in order to emphasize where fermions respectively bosons have greater work output. Light-green is used to indicate the negative work output region.

Let us now briefly examine which N-particle Otto engine has the largest work output depending on the temperatures T_h and T_c. In Fig. 5.7 we indicate which $N = 1, 2, 3, 4$ has the largest work output for given temperatures of T_h and T_c, considering an interaction strength of $g = L_h/b$ and a compression ratio of $L_c/L_h = 2$. If we compare with the non-interacting case (see Fig. 4.6) the fermions are seen to qualitatively change very little. The bosons, on the other hand, have a more significant change. For the non-interacting case the bosons had the largest work output for the greatest N, at all values of T_h and T_c. But for the interacting case we see that for the lower temperatures, the bosons have a larger work output for smaller N. The plot for the interacting bosons looks qualitatively similar to the plots for the interacting and non-interacting fermions. This is to be expected, as introducing our interaction brings a repulsive element to the bosons now as well. For this reason it also makes sense that the fermions do not change their qualitative behaviour in any significant way when the interaction is introduced, as they already had the effect from the Pauli principle.

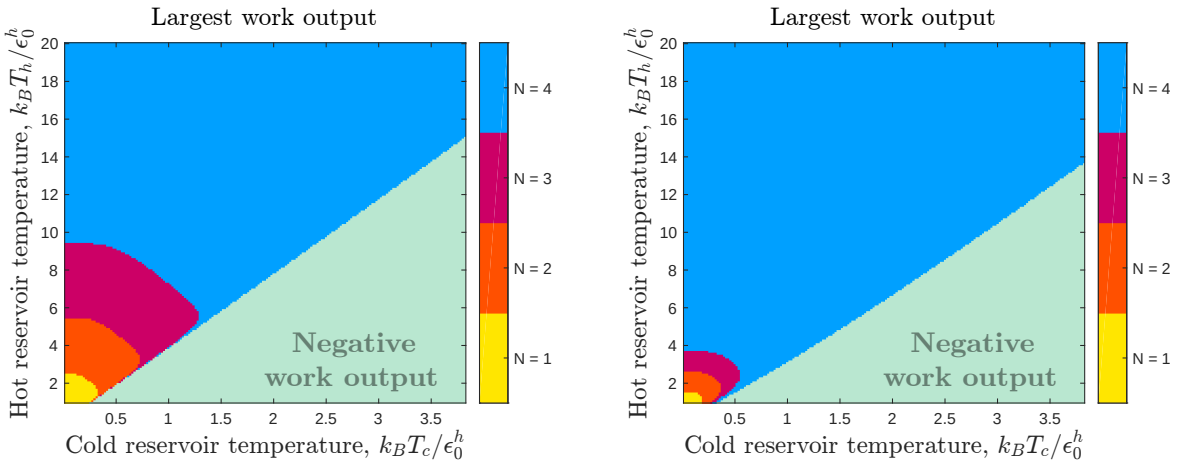

(a) Fermions **(b)** Bosons

Figure 5.7: *Interacting particles.* The plots show which N-particle Otto engine has the largest work output, for $N = 1, 2, 3, 4$, depending on the temperatures of the reservoirs, T_h and T_c. The compression ratio is fixed to $L_c/L_h = 2$. Light-green is used to indicate the negative work output region. The interaction strength is set to $g = L_h/b$.

Let us now look at which N-particle Otto engine has the largest work output *per particle*, plotted in Fig. 5.8. We look at $N = 1, 2, 3, 4$, using an interaction strength of $g = L_h/b$ and a compression ratio of $L_c/L_h = 2$.

Looking at the fermions first, and comparing the interacting case to the non-interacting case (Fig. 4.7a), we see that they look similar. However, there are some apparent differences close to the negative work output region. We see that the temperature region where a given $N > 1$ has largest work output extends with sort of a "tail" going downwards along the negative work output region. This can be a result of the change in the condition for positive work output. For $N = 1$, there will not be any contribution from the interaction, as there is only the one particle, and hence it needs to satisfy $T_h > (L_c/L_h)^2 T_c$, in order to perform positive work. Higher N, which will have a contribution from the interaction, are not subject to the condition $T_h > (L_c/L_h)^2 T_c$ in order to do positive work; and as we saw above it seemed both fermions and bosons had lower bounds than $T_h > (L_c/L_h)^2 T_c$, in order to perform positive work.

Turning to the bosons, we recall that for the non-interacting case (Fig. 4.7b), the work output per particle was largest for $N = 1$ at all temperatures. It seems from Fig. 5.8b that when considering interacting particles, $N > 1$ can have largest work output per particle, if T_c is large enough compared to T_h. One reason for this could be that, as the excitation energies are increased for interacting particles compared to non-interacting ones, they require higher temperature in order to be excited. For sufficiently low values of T_c, we would then have that the work cost of W_c should decrease, for the interacting particles. As the $N = 1$ case is non-interacting, it will have the same work cost while the $N > 1$ cases have a decreased cost. Therefore, if T_c is low enough to make the $N > 1$ cases have smaller W_c than their corresponding non-interacting cases, while T_c is also high enough to give a non-negligible work cost for the $N = 1$ case, it could lead to the $N = 1$ case having a lower work output per particle than the $N > 1$ cases. Increasing the interaction strength further, to e.g. $g = 5L_h/b$, we found that the plot for the bosons looked similar

to the corresponding plot for the fermions (which in turn looked qualitatively similar to the $g = L_h/b$ plot, Fig. 5.8a). This is what we expect, since the fermions' and bosons' excitation energies become closer when the interaction strength is increased.

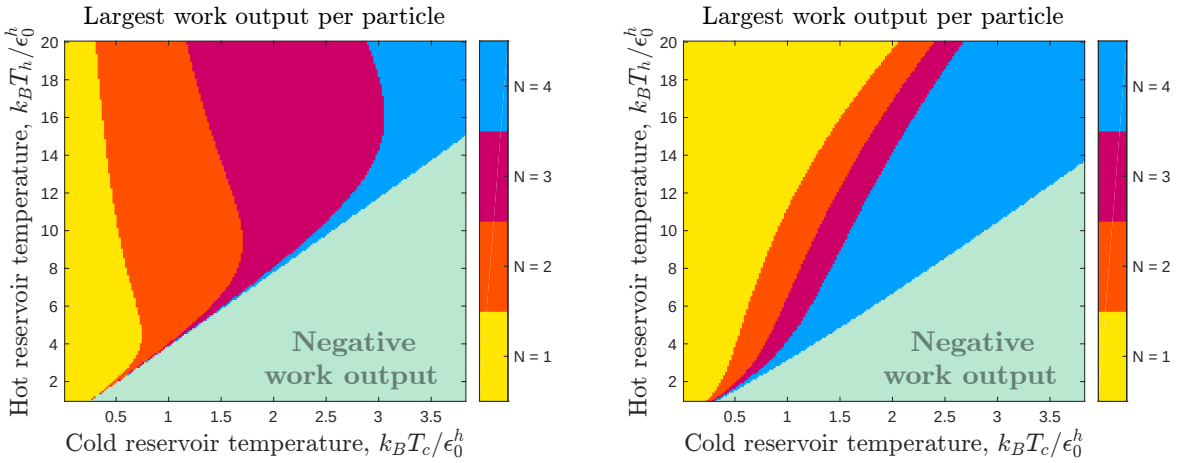

(a) Fermions **(b)** Bosons

Figure 5.8: *Interacting particles.* The plots show which N-particle Otto engine has the largest work output per particle, for $N = 1, 2, 3, 4$, depending on the temperatures of the reservoirs, T_h and T_c. The compression ratio is fixed to $L_c/L_h = 2$. Light-green is used to indicate the negative work output region. The interaction strength is set to $g = L_h/b$.

5.4 Conclusion

We have seen that introducing the two-body interaction between the particles can make a considerable difference compared to the non-interacting case. We here summarize and comment on the observations made.

- We have seen that the interaction allows both fermions and bosons to get higher work output compared to the non-interacting case, if the temperatures of the reservoirs are high enough. For sufficiently low temperatures, the work output can instead decrease. This would be important to take into account when applying the concepts on a possible experimental engine. Depending on the temperature we will run it on, either interacting or non-interacting would be preferable. If we then are looking to run the engine on higher temperatures (as higher temperatures will increase the work output), but still on low enough temperatures such that the system does not reach the classical limit, interacting particles would seem preferable over non-interacting. This could simplify possible experimental set-ups, by being able to use e.g. electrons (which by default interacts with each other through the Coulomb interaction) as the the working medium.

- We saw that the effect of including the interaction is more apparent for bosons than fermions. This can be explained by that the fermions obey the Pauli principle, which forbids them to get in close contact where the interaction has the largest magnitude. Additionally, increasing the interaction strength sufficiently high, fermions and bosons tend to the same work output, when undergoing the Otto engine. This followed since for strong interactions, the interaction will dominate the behaviour of the particles such that bosons and fermions would behave similarly.

- Finally, we saw that the qualitative dependence on particle number was similar for the interacting fermions considered and non-interacting fermions; in that we had similar temperature regions for which particle number yielded the largest work output. For experimental engines, this would just mean that the optimisation with respect to particle number is similar for the interacting and non-interacting fermions. The interacting bosons, we could see, instead had a different dependence on particle number compare to the non-interacting bosons. While for the non-interacting case, it seemed, for any temperatures, more bosons gave a larger work output; the interacting case showed that different particle number had a larger work output at certain lower temperatures (similarly to the interacting and non-interacting fermions).

Chapter 6

Outlook

We have in this thesis looked at a quasi-statically driven Otto engine operating a 1D quantum system confined in an infinite square well. We were interested in the work output of few-body systems, and how the work output change when considering different working media (i.e. classical particles, non-interacting quantum particles and interacting quantum particles). The idea is that this could give us further understanding about what considerations to take into account when constructing experimental engines, and what restrictions there could be for different working media.

We started by examining systems consisting of non-interacting, spin-polarised fermions or bosons. It was found that fermions and bosons had different work output, and we argued that the underlying reason was the different particle statistics and the monotonically increasing energy level spacings of the infinite square well. We further found that for fermions, the optimal particle number to maximize work output or work output per particle depended on the temperatures of the heat reservoirs. Overall, it appeared higher temperatures of the reservoirs favoured higher particle number, which could be explained by that the excitation energies increased as the particle number increased, for the fermions. For the bosons, the work output seemed to increase when adding more particles while the work output per particle seemed to decrease when adding more particles, independent of the temperatures of the heat reservoirs. The reason for this is not as clear compared to the reason for the particle number dependence of the fermions, and needs further study to be explained.

Additionally for non-interacting particles, we found that when considering $N \leq 4$, any N-fermion engine was able to have a larger work output than the corresponding classical case (consisting of 1D, mono-atomic, ideal gas particles), for sufficiently high temperatures of the reservoirs, while for bosons only $N = 1$ and 2 could have a larger work output than the classical case. We again need to investigate more to be able to address why the bosons only have $N = 1$ and 2 with larger work output than the classical case. However, the result that the fermions can have a larger work output than the classical case for any of the N considered, encourage for further studying engines operating quantum particles, in hopes that the quantum domain could be utilised to improve engine performance.

We moved on to include a two-body interaction in our Hamiltonian, taken to be of the same form as an effectively 1D Coulomb interaction for a system under strong cylindrical confinement. We found that it allowed both fermions and bosons to obtain a larger

work output than the non-interacting case, depending on the temperatures of the heat reservoir. It seemed that due to the Pauli principle restricting fermions from getting into close contact with each other, the effect of the interaction was (for lower values of the interaction strength) more visible on the bosons. We also found that for a sufficiently strong interaction, fermions' and bosons' energy levels tended to the same values, and therefore their work output also did; indicating that the interaction dominates the particle behaviour at this point.

The qualitative temperature dependence for which N-particle engine has the largest work output, was similar for the interacting and the non-interacting fermions. For the interacting bosons, we found that they started to have similar temperature dependence as the (interacting and non-interacting) fermions. In case we are setting up for an experimental engine, these results then tell us to keep in mind that the optimal number of particles in the system depends on which temperatures of the reservoirs we are using.

There are several directions to continue the study of the quantum systems undergoing the Otto cycle we have examined. We could continue to study the same set-ups more thoroughly, and try to find more precise ways to deal with the analysis of the results, in order to understand them more quantitatively. Specifically, we could try to assess to what degree we can, for our results, identify the two-body interaction we use as the effective 1D Coulomb interaction. As we discuss in Appendix C, it does seem possible that, at least the interacting fermions we study could have the two-body interaction identified as the Coulomb interaction. Since we found that the interacting particles were able to have a larger work output than non-interacting ones (and hence also larger work output than classical, ideal gas particles), at sufficiently high temperatures, it would then be of experimental interest to be able to use Coulomb interacting particles, such as electrons, not only because they are common in nature, but also as they could be a competitive working medium.

Furthermore, we could also study the efficiency, defined as

$$\eta = \frac{W}{Q_{\text{in}}} = 1 - \frac{Q_{\text{out}}}{Q_{\text{in}}}\,,$$

where W is the work and $Q_{\text{in(out)}}$ is the heat transfer into (out of) the system. We could investigate the efficiency in the same way as the work output has been examined in this thesis, and try to optimize the efficiency and work output together.

Another continuation of the thesis would be to look at the effect from different trapping potentials. In Ref. [5], they look at quasi-statically driven Otto engines and how the work output ratio of non-interacting fermions and bosons compare for different trapping potentials. They find that the work output ratio in the infinite square well and the triangular potential show opposite behaviour; for fixed T_c, fermions were found to have a larger work output than bosons at high values of T_h in the infinite square well, while they have a larger work output than bosons for low T_h in the triangular potential. The underlying reason is that the infinite square well has monotonically increasing energy level spacings, while the triangular potential has monotonically decreasing energy level spacings. We could then expect that, using a triangular potential will make fermions relate to bosons in a similar way as how bosons relate to fermions in the infinite square

well. We could then, for example, look into this by examining a system with a triangular potential in a similar way as to how we have studied the infinite square well in this thesis.

In Ref. [5], they also looked at the harmonic oscillator, where fermions and bosons are shown to have the same work output (for non-interacting particles), due to the constant energy level spacings. It could then be interesting to investigate how the work output and work output per particle change with particle number and compression ratio; and what would happen when introducing an interaction.

A final suggestion, and probably the most interesting direction to continue the work in terms of studying more realistic processes, would be to look at the Otto engine operating under finite-time. The discussion so far has been for a quasi-statically driven Otto engine, but moving onwards to finite-time would open up a lot more analysis and optimization questions (in e.g. Ref. [6], they look at sudden-quench driving for bosons in the harmonic oscillator, interacting through an inverse-square pairwise potential). Specifically, we would be able to look at the power output (work output per unit of time) of the engine, and could thus consider more realistic models of the Otto engine. Finite-time studies allow to investigate how the expansion and compression speed would affect the power output, work output and efficiency of the engine, all of which we could look into how to optimize simultaneously. Then there is also the question of how to couple to the heat reservoirs in finite-time, and what effects that should be taken into consideration as this is done.

Bibliography

[1] Abah, O. *et al.* Single-ion heat engine at maximum power. *Physical Review Letters* **109** (2012). https://arxiv.org/abs/1205.1362.

[2] Roßnagel, J. *et al.* A single-atom heat engine. *Science* **352** (2016). https://arxiv.org/abs/1510.03681.

[3] Kieu, T. D. Quantum heat engines, the second law and maxwell's daemon. *The European Physical Journal D-Atomic, Molecular, Optical and Plasma Physics* **39** (2006). https://arxiv.org/abs/quant-ph/0311157.

[4] Quan, H., Liu, Y. X., Sun, C. & Nori, F. Quantum thermodynamic cycles and quantum heat engines. *Physical Review E* **76** (2007). https://arxiv.org/abs/quant-ph/0611275.

[5] Zheng, Y. & Poletti, D. Quantum statistics and the performance of engine cycles. *Physical Review E* **92** (2015). https://arxiv.org/abs/1504.02183.

[6] Jaramillo, J., Beau, M. & del Campo, A. Quantum supremacy of many-particle thermal machines. *New Journal of Physics* **18** (2016). https://arxiv.org/abs/1510.04633.

[7] Benson, H. *University physics* (John Wiley & Sons Inc., 1996), revised edn.

[8] Schroeder, D. V. *An introduction to thermal physics* (Addison Wesley Longman, 1999).

[9] Young, H. D. & Freedman, R. A. *University Physics with Modern Physics* (Pearson Education Inc., 2015), 14th edn.

[10] Chandler, D. *Introduction to modern statistical mechanics* (Oxford University Press, 1987), 1st edn.

[11] Sakurai, J. J. & Napolitano, J. J. *Modern Quantum Mechanics* (Pearson, 2010), 2nd edn.

[12] Fetter, A. L. & Walecka, J. D. *Quantum theory of many-particle systems* (Courier Corporation, 2003).

[13] Gross, E. K. U., Runge, E. & Heinonen, O. *Many-particle theory* (Institute of Physics Publishing, 1991).

[14] Lapack library, http://www.netlib.org/lapack/.

[15] Bengtsson, J. private communication (2016).

[16] de Boor, C. *A practical guide to splines* (Springer-Verlag New York, 1978).

[17] Bednarek, S., Szafran, B., Chwiej, T. & Adamowski, J. Effective interaction for charge carriers confined in quasi-one-dimensional nanostructures. *Phys. Rev. B* **68**, 045328 (2003).

[18] Wang, Y., Miao, W.-D. & Zhai, L.-X. An effective screened coulomb interaction in a quasi-one-dimensional system. *Physics Letters A* **378** (2014).

[19] Zhang, A., Zheng, G. & Lieber, C. *Nanowires: Building Blocks for Nanoscience and Nanotechnology* (Springer, 2016).

[20] Nag library manual (f08gaf (dspev) routine), `https://www.nag.co.uk/numeric/fl/nagdoc_latest/pdf/f08/f08gaf.pdf`.

[21] Abedinpour, S. H., Polini, M., Xianlong, G. & Tosi, M. Density-functional theory of inhomogeneous electron systems in thin quantum wires. *The European Physical Journal B* **56** (2007). `https://arxiv.org/abs/cond-mat/0611737`.

Appendix A

Numerical parameters

For the interacting particles in Ch.5 we cannot obtain analytical solutions and therefore use the configuration interaction method with a B-spline basis, as discussed in Sect. 3.2 and 3.3. Throughout this thesis, we have set the order of the B-splines to 5 and used an equidistant knot point distribution. The number of B-splines then determine the single-particle basis size, which in turn determines the many-particle basis size (Note that the number of B-splines is determined by the relation: (Number of B-splines = Number of Knot Points + B-spline order − 4)).

As the number of many-particle states grow very rapidly as the particle number, N, is increased, we have to consider a smaller number of B-splines for the larger N. Further, we have also decreased the number of B-splines for simulations where we look at how the energy levels or the work output develops over a range of interaction strengths or well lengths (or equivalently compression ratios). This is because we have to run the full calculations for each interaction strength and each well length (compression ratio), and thus the runtime increases compared to when considering only one value for the interaction strength and the well length (compression ratio).

For the surface plots, Figs. 5.4, 5.6, 5.7, 5.8 and for Fig. 5.5a, we plot for fixed values of the interaction strength and the compression ratio. We have used 100 B-splines for $N = 1$, 100 B-splines for $N = 2$, 80 B-splines for $N = 3$ and 40 B-splines for $N = 4$.

For Figs. 5.1, 5.2 and 5.5b, we plot against interaction strength for $N = 3$, and have used 50 B-splines. Finally, for Fig. 5.3 we plot against the well length (compression ratio) for $N = 3$, and have used 60 B-splines.

Convergence checks

To verify the validity of our results we need to examine if they have converged to their "true" values. If we assume we have implemented the problem correctly, we need to be sure we choose a large enough basis in order to get accurate results. For this thesis, we have compared the quantities we have plotted in the figures (with the number of B-splines as specified above) to runs with lower number of B-splines, that approximately correspond to halving the many-particle basis sizes. We then first checked that the produced figures for the lower and the higher B-spline numbers looked similar to the eye. Second, we examined the relative difference between the quantities in the figures for the lower and

the higher B-spline numbers, and checked that it was $\lesssim 0.005$.[1]

We would also like to note that, even though we have analytical energy levels for the non-interacting case, we need to make sure that we use enough of them such that the results are converged. We therefore, also for the non-interacting case, check that the results do not change as the amount of levels are lowered.

[1]Note that for cases where the values of T_h and T_c implied that the work output was very close to the border of becoming negative, the values of the work output can be very low. This then means that the numerical accuracy might not be the best, and we could therefore have points here where the relative difference exceeded 0.005. However, we can fairly certainly ignore these, in case we see that these points are just confined to being very close to the border of negative work output values. In a similar sense, we could also expect that the relative difference can become a bit larger in case we look at very low T_h and T_c, where the work output again is very low.

Appendix B

Derivation of the positive-work condition for non-interacting particles

The positive-work condition, $T_h > \nu^2 T_c$, holds for a system of N non-interacting particles undergoing the Otto cycle, given that their energy levels exhibit the scaling property $E_n^h/E_n^c = \nu^2$. We will here derive this positive-work condition, closely following the derivation in Ref. [3] where it was done for the single-particle case (i.e. $N = 1$).

For non-interacting particles, the many-particle energy levels are the sum of the single-particle energy levels populated by each particle. Hence, we have

$$E_n^i = \sum_k \epsilon_k^i m_{n,k} \,, \tag{B.1}$$

where ϵ_k^i is the kth single-particle energy level and $m_{n,k}$ is the occupation-number of the kth single-particle state for the nth many-particle energy level.

Since our system exhibits the scaling property, we have that the single-particle energy levels satisfy $\epsilon_k^h/\epsilon_k^c = \nu^2$. Specifically, the level dependence of the energies should then factor out, such that we have $\epsilon_k^i = \zeta_i f(k)$, where, e.g., for the infinite square well $\zeta_i = \hbar^2\pi^2/(2mL_i^2)$ and $f(k) = (k-1)^2$, $k = 0, 1, 2, \ldots$. We can now express (B.1) as

$$E_n^i = \zeta_i \sum_k f(k) m_{n,k} = \zeta_i F(n) \,, \tag{B.2}$$

where we have defined the function

$$F(n) \equiv \sum_k f(k) m_{n,k} \,.$$

If we now plug (B.2) into the expression for the work output (see (2.12)), and use that our occupation-probabilities are Boltzmann-factors, we obtain

$$W = (\zeta_h - \zeta_c) \sum_n F(n) \left(\frac{\mathrm{e}^{-\zeta_h F(n)/(k_B T_h)}}{Z_h} - \frac{\mathrm{e}^{-\zeta_c F(n)/(k_B T_c)}}{Z_c} \right) . \tag{B.3}$$

Now, set $\gamma_i = \zeta_i/(k_B T_i)$ and let $y = \gamma_c - \gamma_h$. We can then rewrite (B.3) as a function of y,

$$W(y) = (\zeta_h - \zeta_c) \sum_n F(n) \left(\frac{\mathrm{e}^{-\gamma_h F(n)}}{Z_h} - \frac{\mathrm{e}^{-(y+\gamma_h)F(n)}}{Z_c} \right) . \tag{B.4}$$

Note that

$$\sum_n F(n) \mathrm{e}^{-(y+\gamma_h)F(n)} = \sum_n \frac{\partial}{\partial y} \mathrm{e}^{-(y+\gamma_h)F(n)} = \frac{\partial Z_c}{\partial y} .$$

Thus, taking the partial derivative of (B.4), with respect to y, yields

$$\begin{aligned}
\frac{\partial W}{\partial y} &= (\zeta_h - \zeta_c) \frac{\partial}{\partial y} \Big(- Z_c^{-1} \sum_n F(n) \mathrm{e}^{-(y+\gamma_h)F(n)} \Big) \\
&= (\zeta_h - \zeta_c) \left(Z_c^{-2} \frac{\partial Z_c}{\partial y} \sum_n F(n) \mathrm{e}^{-(y+\gamma_h)F(n)} - Z_c^{-1} \sum_n F(n) \frac{\partial}{\partial y} \mathrm{e}^{-(y+\gamma_h)F(n)} \right) \\
&= (\zeta_h - \zeta_c) \, Z_c^{-1} \sum_n \mathrm{e}^{-(y+\gamma_h)F(n)} \left(F(n) - \left(Z_c^{-1} \sum_{n'} F(n') \mathrm{e}^{-(y+\gamma_h)F(n')} \right) \right)^2 > 0 .
\end{aligned}$$

That $\partial W/\partial y > 0$, follows from $\zeta_h - \zeta_c > 0$ and that in the last line the sum is over squared terms.

With $\partial W/\partial y > 0$, we have that $W(y)$ is a strictly increasing function of y. Further, plugging in $y = 0$ in (B.4), we obtain $W(0) = 0$. Thus, $W > 0$ only when $y > 0$. Consequently, using that $\zeta_h/\zeta_c = \nu^2$,

$$y > 0 \;\; \Rightarrow \;\; \gamma_c > \gamma_h \;\; \Rightarrow \;\; T_h > \frac{\zeta_h}{\zeta_c} T_c = \nu^2 T_c ,$$

which is the condition for positive work output we wanted to show.

Appendix C

Interpretation of the two-body interaction

We will in this chapter discuss the validity of interpreting the two-body interaction (3.22), i.e.

$$v(x_i, x_j) = \frac{\sqrt{\pi} q^2}{2\kappa b} \mathrm{erfcx}\left(\frac{|x_i - x_j|}{2b} \right), \tag{C.1}$$

as an effective 1D Coulomb interaction for our results. As we discussed in Sect. 3.4.2, we can only take (C.1) as an effective 1D Coulomb interaction for a 3D system that has a sufficiently strong, cylindrical confinement in its transverse direction (the derivation is done below, in Appendix D). Increasing the confinement strength was equivalent to decrease b, since the oscillator frequency, $\omega_\perp$, deciding the confinement strength, was given by $\omega_\perp = \hbar/(2mb^2)$. The transverse direction will become smaller and smaller as b is decreased, so that in the limit $b \to 0$, the effective 1D system will be truly 1D. If the results we obtained do not change much when decreasing b, we could imagine that it indicates that the transverse confinement is strong enough for the interaction (C.1) to be identified with the effective 1D Coulomb interaction.

Let us start by compare the potential energy of the two-body interaction (C.1), for different values of b, with the Coulomb potential energy in the 1D limit, $v_C = q^2\kappa^{-1}/x$ (see also Ref. [17], where they do a similar comparison). In Fig. C.1 we plot the potential energy against inter-particle distance (in units of a reference length L), for the Coulomb potential, $v_C = q^2\kappa^{-1}/x$, and the two-body interaction (C.1) for $b = 0.05, 0.005$ and 0.0005 (in units of L). We see that for the larger distances plotted, ($x \sim 0.1L$), all curves tend to the same value, implying (C.1) correctly resembles the Coulomb interaction for all the b's here. However, as the distance is decreased, we see that the higher the value of b is for (C.1), the faster the curve falls off from the Coulomb interaction (if we were to increase the values on the y-axis, we would also see that the $b = 0.0005L$ case moves away from the Coulomb interaction).

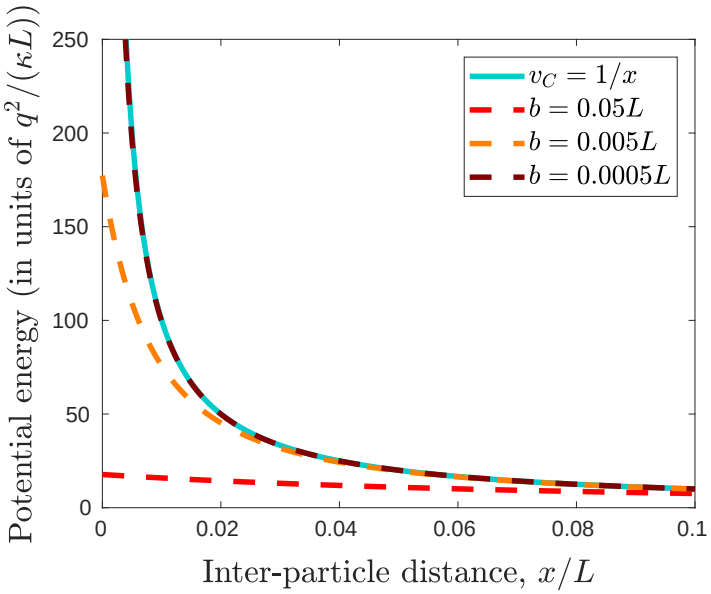

Figure C.1: The potential energy (in units of $q^2/(\kappa L)$) plotted against inter-particle distance x (in units of some reference length L). The solid, light-blue curve plots the Coulomb potential energy, while the dashed curves plot the two-body interaction (C.1) for $b = 0.05, 0.005$ and 0.0005 (in units of L).

Now let us see how different b affect the energy levels and work output for fermions respectively bosons, interacting through (C.1). In Fig. C.2a, we plot Fig. 5.1 again[1], which looks at the lowest excitation energies for three fermions and three bosons, plotted against the interaction strength g, and using $b = 0.005L$. We compare it with Fig. C.2b, having the same set-up, but using $b = 0.0005L$. We see that the qualitative behaviour is similar. However, we can note that for the lower value, $b = 0.0005L$, the bosons' levels tend to the fermions' levels faster, i.e. for lower g. We can actually see that the relative difference between the energy levels using $b = 0.005L$ and $b = 0.0005L$ is a a lot larger for the bosons than the fermions, see Figs. C.3a and C.3b. For the fermions, we have an overall relative difference that is below 0.003, for the levels plotted, while the bosons have all levels above 0.05 for many of the interaction strengths.[2] We could think that this difference between the fermions and bosons arises due to the fact that, since the fermions obey the Pauli principle, they are not allowed in contact; and hence, the interaction at zero inter-particle distance is irrelevant for the fermions. It is also at the very short inter-particle distances the interaction (C.1) differs the most when changing b, as we saw in Fig. C.1. And since the bosons have no restriction on whether they are allowed into contact or not, we could expect them to be more sensitive to changes of the potential at the short inter-particle distances.

[1] Just for clarity, we consider a smaller region of g values here.

[2] Additionally, it was also found that comparing two lower values of b than the ones considered here, didn't seem to improve the situation for the bosons to an acceptable degree (by which we would like to have a relative difference of less than, our around 0.005).

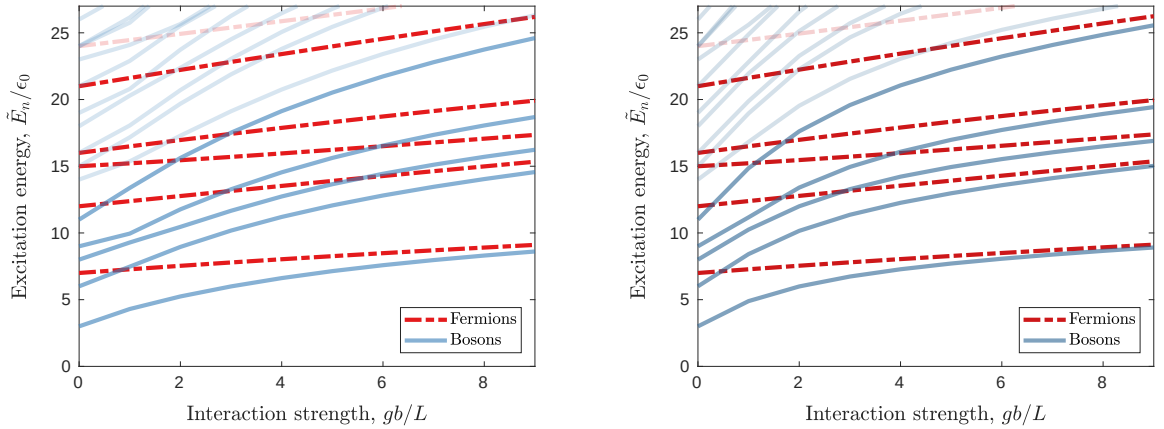

(a) $b = 0.005L$ **(b)** $b = 0.0005L$

Figure C.2: *Interacting particles.* Excitation energy to the nth many-particle energy level versus the interaction strength, g, for (a) $b = 0.005L$ and (b) $b = 0.0005L$. The plots consider three fermions and three bosons. The lines for the 6th and higher excitation states are faded to make the images more clear.

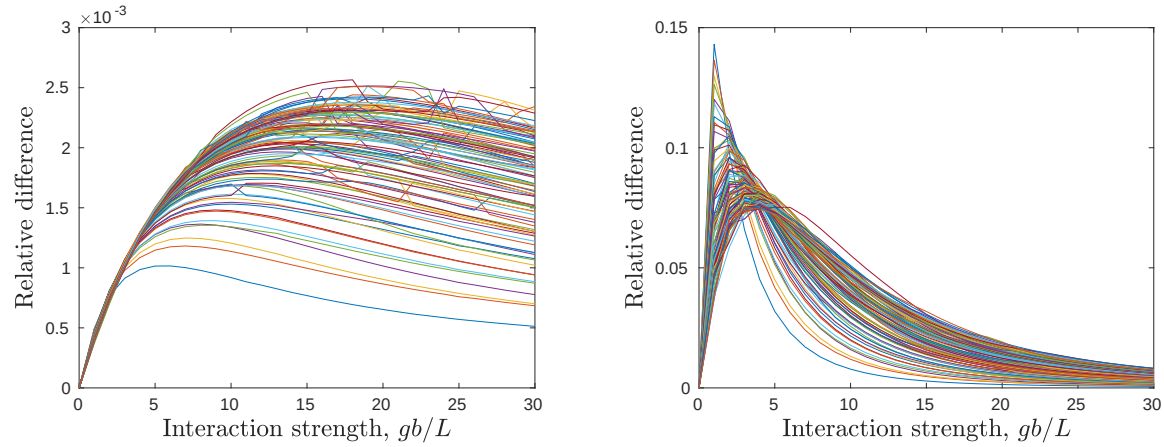

(a) Fermions **(b)** Bosons

Figure C.3: *Interacting particles.* Relative difference between the excitation energies using $b = 0.005L$ and $b = 0.0005L$, for (a) fermions and (b) bosons. The plots consider $N = 3$ and look at the first 100 levels for a range of interaction strengths, g. Note: we used 50 B-splines to calculate the energy levels for the respective cases considered in the plots.

Let us finally look at the relative difference between the work output using $b = 0.005L_h$ and $b = 0.0005L_h$. In Fig. C.4, the relative difference is plotted for three fermions, Fig. C.4a, and three bosons, Fig. C.4b, for a fixed interaction strength $g = L_h/b$. We see that the fermions have a fairly low relative difference between $b = 0.005L_h$ and $b = 0.0005L_h$, only

reaching above 0.005 close to the negative work output region.[3] Looking at the bosons, we do instead see a much larger relative difference than compared to the fermions (just as for the energy levels in Fig. C.3).

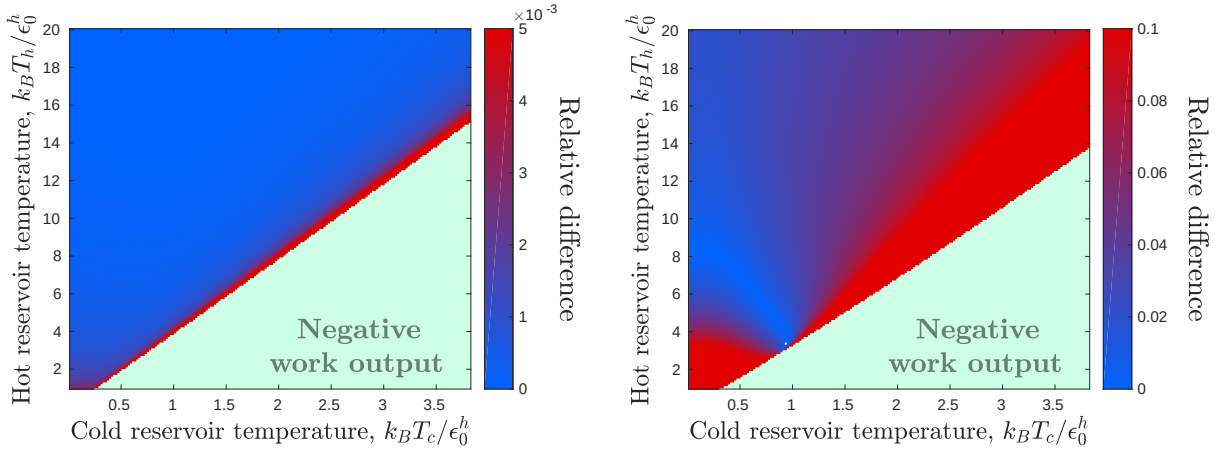

(a) Fermions **(b)** Bosons

Figure C.4: *Interacting particles.* Relative difference between the work output using $b = 0.005L$ and $b = 0.0005L$, for (a) fermions and (b) bosons. The plots consider $N = 3$ and an interaction strength of $g = L_h/b$. Note: we used 60 B-splines when calculating the energy levels for the respective cases considered in the plots.

So to conclude this appendix chapter: we have seen that the interaction (C.1) is affected the most at short inter-particle distances, when the confinement strength is increased, i.e. b decreased. It can be argued that for this reason, we find fermions more stable to changes in b than bosons (since the fermions are not allowed in contact due to the Pauli principle, and hence not as sensitive to changes in the behaviour at short inter-particle distances). From the examination above, it would seem that for the fermions, we possibly could identify the interaction (C.1) as an effective 1D Coulomb interaction. For the bosons, however, it would not appear to be the case. Nonetheless, in regards to experimental settings, Coulomb interacting fermions would be of high interest to use anyway, as they could be realised by electrons. We should still, for both fermions and bosons, do further investigations in order to be sure how large the difference is between applying an actual 3D Coulomb interaction, and using the effective 1D interaction (C.1). In Ref. [17], they compare the effective 1D interaction (C.1) with the results for using the full 3D Coulomb interaction and solving the system by variational calculations on a trial wave function. Something similar might be possible in our case (note though that Ref. [17] only looks at the ground state energies of the systems they consider).

[3] Close to the negative work output region, the work output becomes very low and hence the numerical precision can drop in the calculations. We could from that then expect a larger relative difference here (but that does not rule out that there, in fact, could be a larger relative difference here because of some other reason).

Appendix D

Derivation of the effective 1D Coulomb interaction

Here we will derive the form of the effective 1D Coulomb interaction, discussed in Sect. 3.4.2 and given by (3.22), i.e.

$$v(x_i, x_j) = g\,\frac{\hbar^2}{mL_h^2}\,\mathrm{erfcx}\!\left(\frac{|x_i - x_j|}{2b}\right), \tag{D.1}$$

where g is an interaction strength, $\mathrm{erfcx}(x)$ is the exponentially scaled error function, $\mathrm{erfcx}(x) = \exp(x^2)\,\mathrm{erfc}(x)$, and $\mathrm{erfc}(x)$ is the complementary error function, $\mathrm{erfc}(x) = 2\pi^{-1/2}\int_x^\infty dt\,\exp(-t^2)$. For the derivation, we follow Ref. [18], where it is done for a screened Coulomb interaction for a two electron system. We will also start off with a screened Coulomb interaction and then let the screening parameter go to zero in the end (to end up with the unscreened Coulomb interaction).[1] Article [21] was the main source used in this thesis for the idea of using the effective 1D Coulomb interaction, (3.22).

Introducing the screening, the Coulomb interaction will take the form

$$v(\mathbf{r}_i, \mathbf{r}_j) = \frac{q^2 \mathrm{e}^{\lambda|\mathbf{r}_i - \mathbf{r}_j|}}{\kappa|\mathbf{r}_i - \mathbf{r}_j|}\,,$$

where λ is the screening parameter (which will be set to zero at the end to obtain the unscreened Coulomb interaction), q the charge of the particles, κ the background permittivity and $\mathbf{r}_i = (x_i, y_i, z_i)$.

The energy term due to the Coulomb interaction between particles i and j is given by

$$E_\mathrm{C} = \int d^3\mathbf{r}_1 \cdots d^3\mathbf{r}_N\, \frac{q^2 \mathrm{e}^{\lambda|\mathbf{r}_i - \mathbf{r}_j|}}{\kappa|\mathbf{r}_i - \mathbf{r}_j|}\,|\Psi(\mathbf{r}_1, \ldots \mathbf{r}_N)|^2\,, \tag{D.2}$$

where

$$\Psi(\mathbf{r}_1, \ldots \mathbf{r}_N) = \psi(y_1, z_1)\cdots\psi(y_N, z_N)\Phi(x_1, \ldots, x_N)\,, \tag{D.3}$$

with

$$\psi(y_n, z_n) = \frac{\mathrm{e}^{-(y_n^2 + z_n^2)/4b^2}}{(2\pi b^2)^{1/2}}\,, \tag{D.4}$$

[1] The screening is introduced in order to be able to Fourier transform the Coulomb interaction without divergences arising.

as discussed in Sect. 3.4.2. Note that we are working under the assumption that the system is under a sufficiently strong cylindrical confinement in the yz-plane, such that the approximation (D.3) is fine.

We want to start by Fourier transforming each of the terms in (D.2). For a function $f(\mathbf{r})$, where $\mathbf{r}$ is an n-dimensional vector, its Fourier transform, $F(\mathbf{k})$, is given by

$$F(\mathbf{k}) = \frac{1}{(2\pi)^n} \int d^n\mathbf{r}\, f(\mathbf{r})\, \mathrm{e}^{-i\mathbf{k}\cdot\mathbf{r}}\,, \tag{D.5}$$

and the inverse Fourier transform by

$$f(\mathbf{r}) = \int d^n\mathbf{k}\, F(\mathbf{k})\, \mathrm{e}^{i\mathbf{k}\cdot\mathbf{r}}\,. \tag{D.6}$$

We will denote the Fourier transform of $|\Phi(x_1,\ldots,x_N)|^2$ by $\rho(k_{x_1},\ldots,k_{x_N})$, and the Fourier transform of $|\psi(y_n,z_n)|^2$ by $\rho_\perp(k_{y_n},k_{z_n})$, where $\mathbf{k}_n = (k_{x_n},k_{y_n},k_{z_n})$ are the coordinates in Fourier space corresponding to $\mathbf{r}_n = (x_n,y_n,z_n)$. By applying (D.5) on (D.4), we find

$$\rho_\perp(k_{y_n},k_{z_n}) = \mathrm{e}^{-b^2(k_{y_n}^2+k_{z_n}^2)/2}\,. \tag{D.7}$$

Further, if we denote the Fourier transform of the Coulomb interaction by $\mu(\mathbf{k}_{ij})$, we find

$$\mu(\mathbf{k}_{ij}) = \frac{4\pi q^2}{\kappa(|\mathbf{k}_{ij}|^2+\lambda^2)}\,, \tag{D.8}$$

where we denote $\mathbf{k}_{ij} = (k_{x_{ij}},k_{y_{ij}},k_{y_{ij}})$ as the coordinates in Fourier space corresponding to $(\mathbf{r}_i-\mathbf{r}_j) = (x_i-x_j,y_i-y_j,z_i-z_j)$.

Plugging everything into (D.2), we find

$$\begin{aligned} E_\mathrm{C} = &\left(\prod_m \int d^3\mathbf{r}_m\right)\left(\prod_n \frac{1}{(2\pi)^2}\int dk_{y_n}\,dk_{z_n}\,\rho_\perp(k_{y_n},k_{z_n})\mathrm{e}^{i(y_nk_{y_n}+z_nk_{z_n})}\right) \\ &\times \frac{1}{(2\pi)^3}\int d^3\mathbf{k}_{ij}\,\frac{4\pi q^2}{\epsilon(|\mathbf{k}_{ij}|^2+\lambda^2)}\mathrm{e}^{i\mathbf{k}_{ij}\cdot(\mathbf{r}_i-\mathbf{r}_j)} \\ &\times \frac{1}{(2\pi)^N}\int dk_{x_1}\cdots dk_{x_N}\,\rho(k_{x_1},\ldots,k_{x_N})\mathrm{e}^{i(x_1k_{x_1}+\ldots+x_Nk_{x_N})}\,. \end{aligned} \tag{D.9}$$

To start simplifying (D.9), we can use that the delta-function has the integral representation

$$\frac{1}{(2\pi)^3}\int d^3\mathbf{r}\,\mathrm{e}^{i\mathbf{r}(\mathbf{k}-\mathbf{k}')} = \delta(\mathbf{k}-\mathbf{k}') \equiv \delta(k_x-k_x')\delta(k_y-k_y')\delta(k_z-k_z')\,, \tag{D.10}$$

and identify all delta functions we can find in the expression. For all indices n, except i and j, we have terms like

$$\frac{1}{(2\pi)^3}\int d^3\mathbf{r}_n\,\mathrm{e}^{i\mathbf{r}_n\cdot\mathbf{k}_n} = \delta(k_{x_n})\delta(k_{y_n})\delta(k_{z_n})\,.$$

We can then directly integrate out these delta functions in (D.9), as

$$\begin{aligned}\int dk_{x_n}\, dk_{y_n}\, dk_{z_n}\, \rho_\perp(k_{y_n}, k_{z_n})\rho(k_{x_1}, \ldots, k_{x_n}, \ldots, k_{x_N})\delta(k_{x_n})\delta(k_{y_n})\delta(k_{z_n}) \\ = \rho_\perp(0,0)\rho(k_{x_1}, \ldots, 0, \ldots, k_{x_N}) \\ = \rho(k_{x_1}, \ldots, 0, \ldots, k_{x_N})\,,\end{aligned}$$

where we note that $\rho_\perp(0,0) = 1$, from (D.7).

For the terms with indices i and j, we can identify the delta functions

$$\frac{1}{(2\pi)^3}\int d^3\mathbf{r}_i\, \mathrm{e}^{i\mathbf{r}_i\cdot(\mathbf{k}_i+\mathbf{k}_{ij})}\,\frac{1}{(2\pi)^3}\int d^3\mathbf{r}_j\, \mathrm{e}^{i\mathbf{r}_j\cdot(\mathbf{k}_j-\mathbf{k}_{ij})} = \delta(\mathbf{k}_i+\mathbf{k}_{ij})\delta(\mathbf{k}_j-\mathbf{k}_{ij})\,.$$

Carrying out the integrations over $\mathbf{k}_i$ and $\mathbf{k}_j$ in (D.9), along with the integrations for all other n as discussed above, we are left with

$$E_\mathrm{C} = \frac{1}{2\pi^2}\int d^3\mathbf{k}_{ij}\,\frac{q^2}{\kappa\left(|\mathbf{k}_{ij}|^2+\lambda^2\right)}\rho_\perp(-k_{y_{ij}}, -k_{z_{ij}})\,\rho_\perp(k_{y_{ij}}, k_{z_{ij}})\,\rho(0, \ldots, -k_{x_{ij}}, \ldots, k_{x_{ij}}, \ldots, 0)\,.$$

The wave function along the longitudinal direction $\rho(0, \ldots, -k_{x_{ij}}, \ldots, k_{x_{ij}}, \ldots, 0)$ have non-zero input only for the ith and jth argument, being $-k_{x_{ij}}$ and $k_{x_{ij}}$ respectively. We can simplify the above expression by noting that (D.7) tells us that $\rho_\perp$ is even in both its arguments. Further, we rename the (dummy) variable $\mathbf{k}_{ij} = (k_{x_{ij}}, k_{y_{ij}}, k_{z_{ij}})$ to $\mathbf{k} = (k_x, k_y, k_z)$, for simplicity. We end up with

$$E_\mathrm{C} = \frac{1}{2\pi^2}\int d^3\mathbf{k}\,\frac{q^2}{\kappa\left(|\mathbf{k}|^2+\lambda^2\right)}\rho_\perp(k_y, k_z)^2\,\rho(0, \ldots, -k_x, \ldots, k_x, \ldots, 0)\,.$$

Using the inverse Fourier transform to express $\rho(0, \ldots, -k_x, \ldots, k_x, \ldots, 0)$ as

$$\rho(0, \ldots, -k_x, \ldots, k_x, \ldots, 0) = \int dx_1 \cdots dx_N\, |\Phi(x_1, \ldots, x_N)|^2\, \mathrm{e}^{ik_x(x_i-x_j)}\,,$$

and plugging it into the expression above, yields

$$E_\mathrm{C} = \int dx_1 \cdots dx_N\, |\Phi(x_1, \ldots, x_N)|^2\,\frac{q^2}{2\pi^2\kappa}\int dk_y\, dk_z\, \rho_\perp(k_y, k_z)^2\int dk_x\,\frac{\mathrm{e}^{ik_x(x_i-x_j)}}{k_x^2+(k_y^2+k_z^2+\lambda^2)}\,.$$

The energy term is now on the form of an expectation value, w.r.t. the longitudinal direction (i.e. the x-direction), for a function describing an effective 1D Coulomb interaction, $v(x_i, x_j)$, with the form

$$v(x_i, x_j) = \frac{q^2}{2\pi^2\kappa}\int dk_y\, dk_z\, \rho_\perp(k_y, k_z)^2\int dk_x\,\frac{\mathrm{e}^{ik_x(x_i-x_j)}}{k_x^2+(k_y^2+k_z^2+\lambda^2)}\,.$$

The integral over k_x can be evaluated using Cauchy's residue theorem, by integrating in the complex plane and closing the contour in the upper or lower plane if $x_i - x_j > 0$ or

$x_i - x_j < 0$ respectively; note that the poles of the integrand are $k_x = \pm i\sqrt{k_y^2 + k_z^2 + \lambda^2}$. We are left with

$$v(x_i, x_j) = \frac{q^2}{2\pi\kappa} \int dk_y\, dk_z\, \frac{\mathrm{e}^{-\sqrt{k_y^2+k_z^2+\lambda^2}|x_i - x_j|}}{\sqrt{k_y^2 + k_z^2 + \lambda^2}} \mathrm{e}^{-b^2(k_y^2+k_z^2)}\,,$$

where we plugged in the explicit expression for $\rho_\perp$, (D.4). Changing (k_x, k_y) to polar coordinates (k_r, θ) and integrating out θ, we obtain

$$v(x_i, x_j) = \frac{q^2}{\kappa} \int dk_r\, \frac{r}{\sqrt{r^2 + \lambda^2}}\, \mathrm{e}^{-\sqrt{r^2+\lambda^2}|x_i - x_j|}\, \mathrm{e}^{-b^2 r^2}\,.$$

Performing the variable transformation $k_r \to k = b\sqrt{k_r^2 + \lambda^2} + |x_i - x_j|/(2b)$, we find

$$v(x_i, x_j) = \frac{q^2}{\kappa b} \mathrm{e}^{\lambda^2 b^2} \mathrm{e}^{|x_i - x_j|^2/(4b^2)} \int\limits_{|x_i - x_j|/(2b) + \lambda b}^{\infty} dk\, \mathrm{e}^{-k^2}\,.$$

This finally gives us

$$v(x_i, x_j) = \frac{\sqrt{\pi} q^2}{2\kappa b}\, \mathrm{e}^{\lambda^2 b^2}\, \mathrm{erfcx}\left(\frac{|x_k - x_l|}{2b} + \lambda b \right).$$

We have hence obtained the desired form of the effective 1D, screened Coulomb interaction, which reduces to (D.1) when letting the screening go to zero, $\lambda \to 0$, and having the interaction strength, g, given by

$$g = \frac{m L_h}{\hbar^2} \frac{\sqrt{\pi} q^2}{2\kappa (b/L_h)}\,.$$